Study and extrapolation of the H $\rightarrow \mu\bar{\mu}$ performances to full Run 3 luminosity and High Luminosity - LHC

submitted in partial fulfilment of the requirements
for the degree of

Master of Science

(FIVE YEARS INTEGRATED PROGRAMME)

in

Physics

by

THAKORE MITANSHU RAJENDRASINH

(Reg. No.: I16PH001)

under the supervision of

Dr. SILVIO DONATO

Researcher, INFN Sez. Pisa, Italy.

&

Prof. ANDREA RIZZI

Associate Professor, University of Pisa & INFN Sez. Pisa, Italy.

&

Dr. AJAY KUMAR RAI

Associate Professor, Department of Physics, S.V.N.I.T.

Department of Physics

Sardar Vallabhbhai National Institute of Technology,

Surat - 395007, Gujarat, India.

MAY 2021

Department of Physics
Sardar Vallabhbhai National Institute of Technology,
(An Institute of National Importance, NIT Act 2007)
Surat - 395007, Gujarat, India.

Declaration of Authenticity

I hereby declare that the dissertation entitled "**Study and extrapolation of the H$\rightarrow \mu\bar{\mu}$ performances to full Run 3 luminosity and High Luminosity - LHC**" is a genuine record of research work carried out by me, and no part of this thesis has been submitted to any university or institution before, for the award of any degree or diploma.

Thakore Mitanshu Rajendrasinh
(I16PH001)
Department of Physics,
S.V.N.I.T., Surat.

Date: 24 May 2021
Place: Surat

Department of Physics
Sardar Vallabhbhai National Institute of Technology,
(An Institute of National Importance, NIT Act 2007)
Surat - 395007, Gujarat, India.

Approval Sheet

Dissertation entitled "**Study and extrapolation of the H$\rightarrow \mu\bar{\mu}$ performances to full Run 3 luminosity and High Luminosity - LHC**" by **Thakore Mitanshu Rajendrasinh (I16PH001)** is approved for the degree of **Master of Science** (Five Years Integrated Programme) in Physics.

24/05/2021

Dr. Vipul Kheraj
(External Examiner)

24/05/21

Dr. Ajay Kumar Rai
(Internal Supervisor)

Dr. Sushil Kumar
(Chairman)

Date:
Place: Surat

Department of Physics
Sardar Vallabhbhai National Institute of Technology,
(An Institute of National Importance, NIT Act 2007)
Surat - 395007, Gujarat, India.

CERTIFICATE

This is to certify that the dissertation entitled "**Study and extrapolation of the $H \to \mu\bar{\mu}$ performances to full Run 3 luminosity and High Luminosity - LHC**" is based on part of research work done by **Mr. Thakore Mitanshu Rajendrasinh** under my guidance and supervision at the Sardar Vallabhbhai National Institute of Technology, Surat(Gujarat), India.

24/05/21

(Internal Supervisor)
Dr. Ajay Kumar Rai
Associate Professor,
Department of Physics,
S.V.N.I.T., Surat.

Date:
Place: Surat

Acknowledgements

Working on this project and writing this dissertation was a roller coaster ride for me. It wasn't relatively easy because of the pandemic. I certainly wouldn't be able to do it if it weren't for some of the most amazing people that helped me throughout this journey.

Firstly, I am highly thankful to my local supervisor Dr. Ajay Kumar Rai, for allowing me to pursue my interest of working in the field of experimental high energy physics at a foreign institute. Also, I will forever be grateful to Dr. Jyothsna Rani Komaragiri of IISc Bengaluru for supporting me in all my endeavors. I wouldn't have got an opportunity to work on this project without her help and support.

I will be highly indebted to Prof. Andrea Rizzi for inviting me to work as a part of his group on this project as a collaborator. He allowed me to fulfill my dream from my high school days of working as a part of a collaboration at CERN. At one point, it seemed almost impossible to me that a foreign master's student like me would be accepted to become a part of such a vast collaboration. My sincere gratitude to Dr. Andrea Venturi, Leader of CMS Pisa Group, for trusting me and having me as a collaborator. Thanks to the staff at INFN PISA for extending their help by providing me with all the resources. I would also like to thank Dr. Nan Lu, one of our CMS collaborators.

To my mother and father, "thank you" will be an understatement if I try to describe how grateful I feel about everything they have done for me. Although they never got an opportunity to pursue their dreams, they always believed in me and gave me the freedom to follow my passion and interests. I hope that someday I will be able to fully explain to them what I was doing while working on this dissertation. Many thanks to my brother Nirmit for all the gifts.

It would be unfair I forget to thank Naman - a very dear friend and also my mentor. He was my source of constant motivation and has been someone I have always looked up to personally and professionally. I also want to thank Aditi for being a great friend throughout my life at SVNIT.

Words will fall short for expressing how grateful I am to Dr. Silvio Donato - the best guide and collaborator that anyone could ever have. Though we hadn't interacted even once before, I accepted the opportunity to work with him; he made me feel comfortable and was very friendly to work with. He was extremely kind and patient with me, especially when I struggled to write the codes. I can't thank him enough for his always available help and support. I owe it all to him.

Abstract

Since the discovery of the Higgs boson in 2012 by the ATLAS and the CMS collaborations at CERN, the interactions of the Higgs boson with the other fundamental particles are continuously studied at different mass scales. However, the first evidence of the interaction between the Higgs boson and muons has only recently been presented by the CMS collaboration in a paper published in September 2020. The CMS paper included searches for the processes in which Higgs boson was produced by all four production modes and combined data of Run 2 and Run 1 at various integrated luminosities and center of mass energies. This dissertation estimates the performance for the future analyses about H$\rightarrow \mu\bar{\mu}$ produced through the Vector Boson Fusion mode to the end of the LHC Run 3 (2024, 300 fb^{-1}) and High Luminosity-LHC (2040, 3000 fb^{-1}) luminosities. A total of 3 $\times 10^8$ simulated events amounting to 26 TB of Monte Carlo data were analyzed, including both signal and background processes. Plots of different variables of the particles are presented for the LHC Run 3 and High Luminosity-LHC analyses. The fit of the original analysis is repeated after having scaled the normalization of samples (both signal and background) to expected luminosities, using the Run 3 and HL-LHC cuts. The results show that with increasing luminosity, there will be an appreciable increase in the significance and decrease in uncertainties on the measurement of the VBF H$\rightarrow \mu\bar{\mu}$ cross section in future analyses.

Contents

List of Figures

List of Tables

Chapter 1

Introduction

Ever since the advent of life on earth, we, the curious beings, have always questioned the phenomena around us. We have always wanted to find out "How stuff works?" or "Why nature behaves in a certain way?". Some questions are perhaps too simple to answer, some take up time to be figured out, and some are too complicated, thus, remain unsolved to date. The mysteries of the universe are continuously being unfolded by breakthroughs on the theoretical and experimental fronts.

Without any doubt, curiosity has been the most prominent driving force for various discoveries. However, the tendency to persistently question our current understanding of nature has also played a significant role in this. For instance, Sir Isaac Newton will always be remembered for discovering gravity and providing the universal law of Gravitation. But we wouldn't have a more profound and generalized theory of gravity - the General Theory of Relativity if Albert Einstein had not questioned Newton's ideas. Similarly, the school students would still be taught that "Atoms are indivisible" if J. J. Thomson hadn't discovered the electron by performing experiments with cathode rays.

Curiosity doesn't have any age. It is a propensity that we humans exhibit from the time we are babies. Human babies are one of the most curious creatures. While playing with toys, they often smash the toys on the floor to find out what is inside them. We, physicists, have likewise taken the inspiration from those babies to study the primary constituents of matter. Yes, smashing particles with each other is the crux behind all particle collider experiments around the world.

At the Large Hadron Collider (LHC), trillions of protons are first accelerated to very high energies. They are then made to collide with each other to produce jets of quarks, leptons, and particles. The information about the scattering particles and the particles produced after collisions is collected using detectors. The Physics and the interactions of these particles are then studied by analyzing the detectors' data. This accumulated data is vast and can only be analyzed using high-end computing devices. It was only through

such collisions that the particles like the quarks - up (u), charm (c), top (t), down (d), strange (s), bottom (b); the $W^{\pm}$ and Z bosons, the gluon, and the Tau (τ) lepton were discovered during the 20^{th} century. However, one of the most fundamental questions - "How an object acquires mass?" was still unanswered for the whole of the 20^{th} century and the first decade of the 21^{st} century.

Some groups of physicists around the world tried to answer this question back in the 1950s-60s. They proposed the existence of a 'field' that penetrates all space, interacts with other particles' fields, and provides them mass. A manifestation of this field is the Higgs Boson particle, whose existence was proposed around the same time. However, it was not until 2012 that the Higgs boson was finally observed in the Compact Muon Solenoid (CMS) and A Toroidal LHC ApparatuS (ATLAS) detector experiments, based on collisions in the LHC at CERN. Since its discovery, physicists worldwide are trying to understand the physics of this particle - its mass, its interaction with other particles, and with itself. This dissertation is also an attempt to investigate the interaction of the Higgs boson with a fundamental particle - the muon.

The muon (μ) is a lepton and has a mass about 200 times that of the electron. Of the various decays of Higgs particle, the $H \rightarrow \mu\bar{\mu}$ decay mode was analyzed by the CMS collaboration, and the results were published recently in 2020. The results were in agreement with the theory.

The rare processes have always been of great interest to particle physicists. For studying such rare processes, there's an inevitable need to increase the number of events. Thus, currently, the LHC and the various detector experiments along its circumference are being upgraded. With the up-gradation, it is expected the number of collisions and events will increase by multiple folds. Also, the frequency of Higgs production at the LHC in those collisions will increase. The detectors are also being modified to record the increased number of collisions with better accuracy and precision. The H$\rightarrow \mu\mu$ is one such rare process with a very low branching ratio. With all the upgrades, it will be exciting to study this process at higher luminosities.

In this dissertation, the expected sensitivities of the analysis of the H$\rightarrow \mu\bar{\mu}$ process at Run 3 luminosity and HL-LHC luminosity are presented. These projections will give an essence of what all can be expected from Run 3 and HL - LHC data.

The document is arranged as follows. Chapter 2 aims at instilling the foundational ideas of high energy physics. Chapter 3 details the LHC and the CMS detector experiment. It also gives a brief idea of all the significant ongoing upgrades at the LHC and the CMS. Various Higgs production and decay mechanisms are discussed in Chapter 4 with

a particular emphasis on the H$\rightarrow \mu\mu$ process. Chapter 5 discusses the research objective and methodology employed for pursuing that objective. The extrapolated results with their interpretations are presented in Chapter 6. Chapter 7 will summarise the results with a combined inference, discuss the research's scope, and also lay out future plans.

Chapter 2

Theoretical Background

2.1 Standard Model of Particle Physics

Standard Model is a theory of fundamental forces built on non - abelian gauge fields.

2.1.1 Development

Quantum Electrodynamics (QED) [1] is a field theory used to describe the interactions between light and matter, more precisely between photons and charged particles. Photons are the quanta that mediate electromagnetic interactions. QED is one of the most accurate theories developed so far, with results confirmed through experiments to a high precision level. At its core, it is an abelian gauge theory with $U(1)$ as the symmetry group.

Around the same time as QED was being developed, Enrico Fermi took inspiration from it to formulate a theory of weak interactions for explaining the continuous energy spectrum obtained for the β^- decay process. It was called the Quantum flavourdynamics (QFD) [2]. The approach was successful at explaining the weak nuclear force and its consequences.

Sheldon Glashow showed that the electromagnetic and the weak nuclear forces are manifestations of a singular force - the electroweak force [3]. Furthermore, Salam [4] and Weinberg [5] embodied the Higgs Mechanism [6] [7] into Glashow's theory. This theory was later called on as the Glashow-Weinberg-Salam Theory.

In 1954, Yang and Mills [8] tried to develop a QED - like gauge theory for non - abelian groups to explain the interactions mediated by the strong force. Not just them, but a large number of physicists contributed towards the development of such a theory. This theory introduced a new quantum number - 'color' charge [9] and was later named Quantum Chromodynamics (QCD). In its modern form, QCD was completed by the discovery of asymptotic freedom [10][11].

Only the electroweak theory, along with two generations of quarks, was first called the Standard Model [12]. Later on, with the inclusion of the QCD and other fundamental particles, it got the form that we have today.

2.1.2 Current status

The Standard Model (SM) has proved time and time again to be one of the most consistent theories mathematically. The prime premise of the theory is the existence of quantum fields whose excitations are particles as we see them. The interactions between matter particles (electromagnetic, weak, and strong force) are modeled to be mediated by particles too. The quantum field theory of interactions is a gauge theory of electroweak (unified version of the electromagnetic and weak force) and strong interactions. Mathematically speaking, the gauge symmetry groups that are involved are SU(3) for the strong force, SU(2) for the weak, and U(1) for electromagnetic interactions. When writing these gauge groups, we subscript them with C, L, and Y, representing the color, left, and hypercharge, respectively. The left charge with the weak gauge symmetry group emphasizes that there are no right-handed neutrino components in nature. Finally, when we amalgamate all these groups, we get the gauge group of the entire standard model:

$$SU(3)_C \times SU(2)_L \times U(1)_Y$$

where the part $SU(2)_L \times U(1)_Y$ represents the gauge symmetry group of the electroweak force also known as GWS(Glashow-Weinberg-Salam) electroweak symmetry group. Particles [13] of the Standard Model can be categorized as:

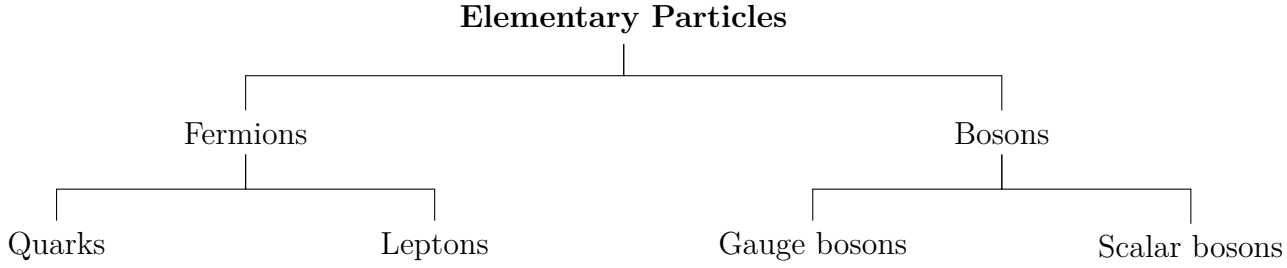

Fermions possess half-integral spins and obey Fermi-Dirac Statistics. Whereas, Bosons have integral spins and obey Bose-Einstein Statistics. In the Standard Model, there are 12 elementary fermions with spin $\frac{1}{2}$. Every fermion has a corresponding anti-particle. Based on their interactions, these fermions can be further categorized as - Quarks and Leptons [14]. There are three generations of fermions. Table 2.1 gives an elaborate classification of the fermions [15]:

	Leptons			Quarks		
	Particles	Q	**mass (in GeV)**	**Particles**	Q	**mass (in GeV)**
First Generation	electron (e^-)	-1	0.0005	down (d)	$-\frac{1}{3}$	0.003
	electron neutrino (ν_e)	0	$< 10^{-9}$	up (u)	$+\frac{2}{3}$	0.005
Second Generation	muon (μ)	-1	0.106	strange (s)	$-\frac{1}{3}$	0.1
	muon neutrino (ν_μ)	0	$< 10^{-9}$	charm (c)	$+\frac{2}{3}$	1.3
Third Generation	tau (τ)	-1	1.78	bottom (b)	$-\frac{1}{3}$	4.5
	tau neutrino (ν_τ)	0	$< 10^{-9}$	top (t)	$+\frac{2}{3}$	174

Table 2.1: Twelve elementary fermions of different generations classified into quarks and leptons. *Source*: [15]:

The characteristic feature of quarks is that they exhibit color charge and therefore interact through strong forces. Quarks also interact via electromagnetic and weak forces. On the contrary, Leptons don't possess any color charge and don't partake in strong interactions. Electron, muon, and tau lepton take part in electromagnetic and weak interactions. The three neutrinos, however, are neutral and only interact via weak forces. They are some of the most elusive particles to be known and even escape detection.

Elementary bosons are exchange particles. Table 2.2 shows the elementary bosons corresponding to the fundamental forces [15]:

Force	**Relative Strength**	**Boson**	**Spin**	**Mass (in GeV)**
Strong	1	Gluon (g)	1	0
Electromagnetism	10^{-3}	Photon (γ)	1	0
Weak	10^{-8}	W boson ($W^\pm$)	1	80.4
		Z boson (Z)	1	91.2
Gravity	10^{-37}	Graviton (G) ?	2	0

Table 2.2: Fundamental forces of nature and their carriers. Their relative strengths are approximated by measuring the force acting between them at a distance of 1 fm. *Source*: [15]

The gluon, photon, $W^\pm$ and Z boson are called gauge bosons since all of them have spin = 1. Like all other fundamental forces, gravity is also believed to be mediated by a hypothesized boson - Graviton. The question mark (?) next to the graviton denotes that there has been no experimental detection or observation of this particle. Apart from gauge bosons, there is another class of elementary bosons called the scalar bosons, with spin = 0. There's only one scalar boson - the Higgs boson (H). The Higgs boson is at the heart of the Standard Model. It is because of the Higgs that the leptons, quarks, $W^\pm$, and Z boson are massive.

In the Standard Model Lagrangian,

$$\mathcal{L} = -\frac{1}{4}F_{\mu\nu}F^{\mu\nu} + i\bar{\psi}\not{D}\psi + h.c. + \bar{\psi}_i y_{ij}\psi_j\phi + h.c. + |D_\mu\phi|^2 - V(\phi) \tag{2.1}$$

we introduce the scalar potential ϕ of a particular vacuum expectation value. This poten-

tial is accountable for the electroweak symmetry breaking and giving mass to the vector bosons. However, when it comes to the fermion sector, the mechanism through which the fermions obtain mass is quite different. They get mass as a result of Yukawa interactions. The fermions' masses depend upon the strength of their interaction with Higgs.

Standard Model describes interactions among particles as a result of the exchanges between the gauge bosons.

2.1.3 Predictions by Standard Model

Standard Model has been one of the most theoretically consistent models so far, successfully making many experimental predictions over the years. These include:

- In 1973, the discovery of the neutral currents [16] in the weak neutral interaction

$$\bar{\nu} + e \rightarrow \bar{\nu} + e$$

  at the Gargamelle Neutrino Experiment at CERN, validated a significant prediction of the Electroweak theory.

- The discovery of the W [17][18] and the Z [19][20] bosons by the UA1 and the UA2 experiments at CERN in 1983.

- The discovery of the top quark in 1975 by the CDF experiment [21] and Dϕ experiment [22] at Tevatron, Fermilab.

- The discovery of τ neutrino [23] by the DONUT experiment at Fermilab in 2000.

- And finally, the discovery of Higgs boson by the CMS [24] and the ATLAS [25] experiments at Large Hadron Collider, CERN in 2012.

2.1.4 Limitations of the Standard Model

The Higgs boson was believed to be the last piece of the puzzle - that physicists were trying to solve for more than four decades. Its discovery was anticipated as the ultimate requirement for proving the Standard Model - a theory capable of describing all particle phenomena.

Despite several accomplishments of the Standard Model, it still has many limitations. These are as follows:

- **Matter - Antimatter Asymmetry:** There's an imbalance in the quantity of matter and anti-matter in our cosmos. It's postulated that the Big Bang should have created equivalent amounts of matter and anti-matter in our universe. However, it's not the case.

- **Dark Matter and Dark Energy:** If we look at the energy budget of the universe, then currently we understand only less than 5% of the matter in the universe. The remainder is Dark Matter ($\sim 24\%$) and Dark Energy ($\sim 71\%$). The standard model doesn't give any information about Dark Matter or Dark Energy.

- **Neutrino Masses:** The neutrinos in the Standard Model are 'massless.' However, with the discovery of the neutrino oscillations by the Super - Kamiokande Collaboration [26] and the Sudbury Neutrino Observatory [27], it was concluded that neutrinos must have non-zero masses. Thus, the Standard Model fails to explain the reason behind the masses of the neutrinos.

- **Exclusion of Gravitation:** The Standard Model doesn't incorporate the Gravitational force. Although an exchange particle for mediating Gravity has been hypothesized - the Graviton, it hasn't been discovered yet.

- **Hierarchy problem:** If we look at Table 2.2, then there's a huge difference between the strengths of forces of nature. The standard Model doesn't explain this disparity between the forces' relative strengths.

Thus, there ought to be physics beyond the Standard Model to account for the phenomena that we observe and yet couldn't explain.

2.2 The Higgs boson

In the GWS theory, to describe the non-zero masses of vector gauge bosons, they introduced the spontaneous breaking of the electroweak symmetry between the γ, Z and $W^{\pm}$ bosons. For this, they assigned a vacuum expectation value, v, to a Higgs field, $\langle\phi\rangle$. The Higgs potential energy distribution can be expressed as:

$$V(\phi) \;=\; -\mu^2\phi^\dagger\phi \;+\; \lambda(\phi^\dagger\phi)^2,\;\; \mu^2 > 0,\;\; \lambda > 0 \tag{2.2}$$

and has the shape as shown in figure 2.1

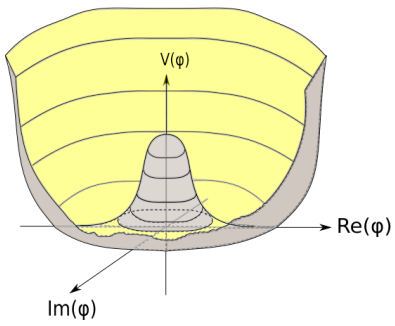

Figure 2.1: Higgs Potential

The Higgs potential is localized around a circle in a complex plane, and it can be defined as

$$\langle \phi \rangle = -v, \qquad v = \frac{\mu^2}{2\lambda} \tag{2.3}$$

The quantity v is called the vacuum expectation value, and its measured value turns out to be 246 GeV. The Higgs field is believed to exist everywhere. It is independent of the presence of any matter.

The excitations of the Higgs field around the minimum value of the Higgs potential describe a bosonic particle with spin = 0. This particle is called the **Higgs boson**. It is without any charge and has a mass of around 125.10 ± 0.14 GeV [28]. It is a very short-lived particle and, upon production, quickly decays into other particles, which will be described further in Chapter 4.

Chapter 3

The LHC and the CMS detector

This chapter gives an insight into the particle accelerator - the Large Hadron collider (LHC) and the Compact Muon Solenoid (CMS) detector installed at one of the LHC points.

3.1 The Large Hadron Collider

The Large Hadron Collider (LHC) [29] is currently the world's largest and most powerful particle collider. Located at the CERN accelerator complex near the borders of two nations - France and Switzerland, the LHC is a 27 km long tunnel situated about 175 m beneath the surface.

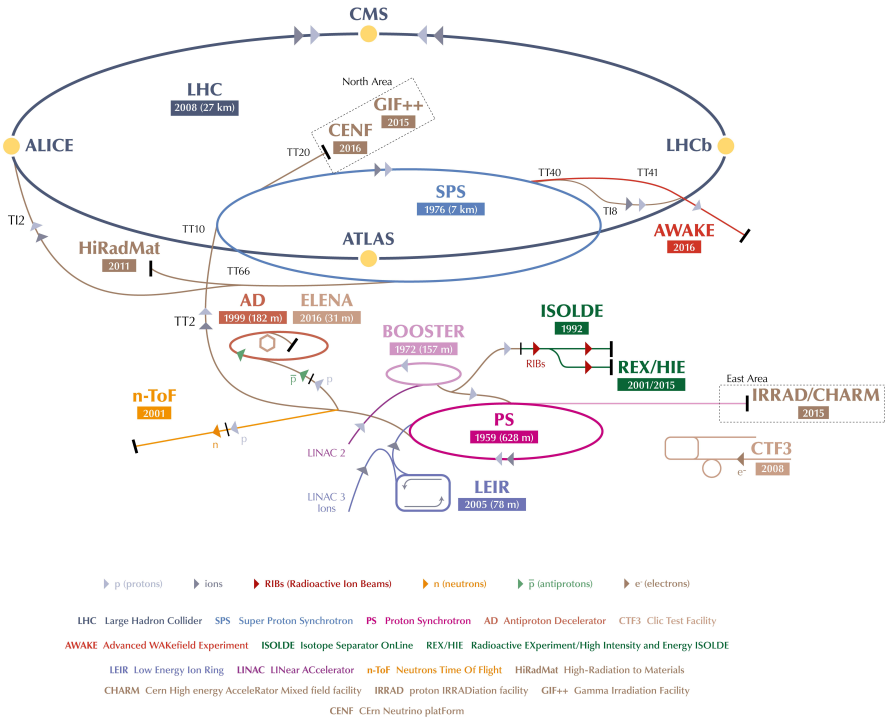

Figure 3.1: CERN Accelerator complex housing the LHC (2016). *Source:* [30]

In figure 3.1, all the rings are particle accelerators varying in size. At LHC, 90% of the time, protons collide with other protons. Sometimes heavier elements like Lead, Oxygen, Xenon, etc., are also collided. These particles are accelerated to very high relativistic speeds. The center of mass energies of the collisions is currently as high as about 14 TeV. For understanding how the LHC works, we will learn about how the protons are accelerated and then collided in the accelerator in the next section.

3.1.1 Acceleration of protons in the LHC

The Hydrogen from the Hydrogen source is pumped into a device called Duoplasmatron, where the generation of plasma state takes place in the presence of a high electric field. In the plasma state, the electrons are stripped from the hydrogen atoms quite easily. At this moment, the protons are not moving at high speeds and need to be accelerated. **Protons are accelerated in the electric field and not in the magnetic field.** There are two beams of protons that are being circulated through LHC.

The protons are accelerated in Linear Accelerator 2 (LINAC 2), whereas the ions are accelerated using LINAC 3. LINAC 2 accelerates proton up to 50 MeV ($\sim$10% of the speed of light). In LINAC 2, the grouping of protons in packets from continuous streams occurs in a radiofrequency cavity using the quadrupole magnets. The proton bunches are then passed through regions of high alternating electric fields, which accelerates them to higher velocities. The electric fields in here change at a frequency that falls into the radiofrequency regime. Thus, it is named the radiofrequency cavity. The controlling of directions and alignment of the beam is achieved through the magnetic fields produced by different kinds of magnets. These include:

- **Dipole Magnets:** These are used for bending the particles in the circular accelerators. They are 15m long and weigh about 28 tonnes each. Using dipole magnets, the beam of protons is deflected by 0.3^{o} per 15 m.
- **Quadrupole Magnets:** These magnets are meant for focusing or defocusing the beam. We need quadrupole magnets to increase the luminosity by keeping them focused since all the beam particles have the same charge and repel each other. The magnetic field inside the quadrupole magnets is hyperbolic, and it works like a lens.
- **Multipoles (sextupoles, octupoles):** Such magnets are mainly used for higher-order corrections.

We need multiple accelerators to boost the speed of protons as we cannot directly accelerate them to the maximum energy at once.

From the hydrogen source, the protons are first injected into the LINAC 2 and accelerated a bit. They are then transferred to the Proton Synchrotron Booster (PS Booster), which increases the energy of protons from 50 MeV to 1.4 GeV and packs more protons together in a bunch. PS Booster is about 20 m in circumference. From the PS Booster, the bunches of protons are transported into the Proton Synchrotron, which is around 628 m long. It further accelerates the protons to 26 GeV energy(∼99.9349015% of the speed of light). The Proton Synchrotron has more than 250 electromagnets which include about 100 dipole magnets. At this stage, the protons are transferred to other experiments which aren't located at the LHC points but in the CERN campus and don't require very high-speed particles.

The proton beams present in the Proton Synchrotron are then injected into the Super Proton Synchrotron (SPS). Its circumference is almost 7 Km and has around 1300 electromagnets that include close to 750 dipole magnets. It can accelerate protons to 450 GeV of energy (∼99.9999989% of the speed of light). Finally, from the SPS, the protons are inserted into the LHC.

With a circumference of about 27 km, the LHC is capable of accelerating protons to energies up to 6.5 TeV (∼99.999999999% of the speed of light). It has the highest number of superconducting electromagnets than other accelerators, including about 1200 dipole electromagnets and nearly 850 quadrupole magnets. These superconducting magnets produce a magnetic field up to 8 T and are maintained at temperatures ∼2 K, making the LHC one of the coldest places on the Earth. Also, there's an ultra-high vacuum inside the LHC of the order 10^{-13} atm, which is stronger than outer space. Such a high level of vacuum is required to ensure no other elements are inside the accelerator.

After accelerating the proton beams to such high speeds, opposite beams are made to collide at multiple points along with the accelerator. Different particle detectors are installed at the beam intersection points to detect and sense the phenomena happening during the collisions. The frequency of these proton collisions is about 40 MHz. The detectors are capable of reading the collisions at 100 kHz. Collisions are recorded at 1 kHz by the trigger systems. The recorded data is then reconstructed and elaborated for future data analysis.

Along the circumference at the LHC points, ten detector experiments are located: ALICE, ATLAS, CMS, LHCb, LHCf, MATHSULA, MilliQan, MOEDAL, TOTEM, and FASER. Out of these, only the CMS and the ATLAS experiments are general-purpose detector experiments. The CMS detector experiment will be discussed in detail in section 3.2.

3.2 The CMS detector

The **C**ompact **M**uon **S**olenoid [31] is a general-purpose detector located at one of the LHC points. It is named 'compact' because of its relatively smaller size than other LHC detectors (ATLAS, ALICE, etc.). It was primarily designed to provide optimal measurements of the muons as they give a relatively 'clean' signal and are often obtained as the end products of many known and unknown processes that we are constantly searching for. The detector is built around a huge single superconducting solenoid capable of generating a magnetic field of slightly less than 4 Tesla. The solenoid is necessary to bend the track of the particles for identifying their charges and measuring their momenta - more the momenta lesser the bending. The size of the detector can be estimated by comparing it to a human figure in figure 3.2.

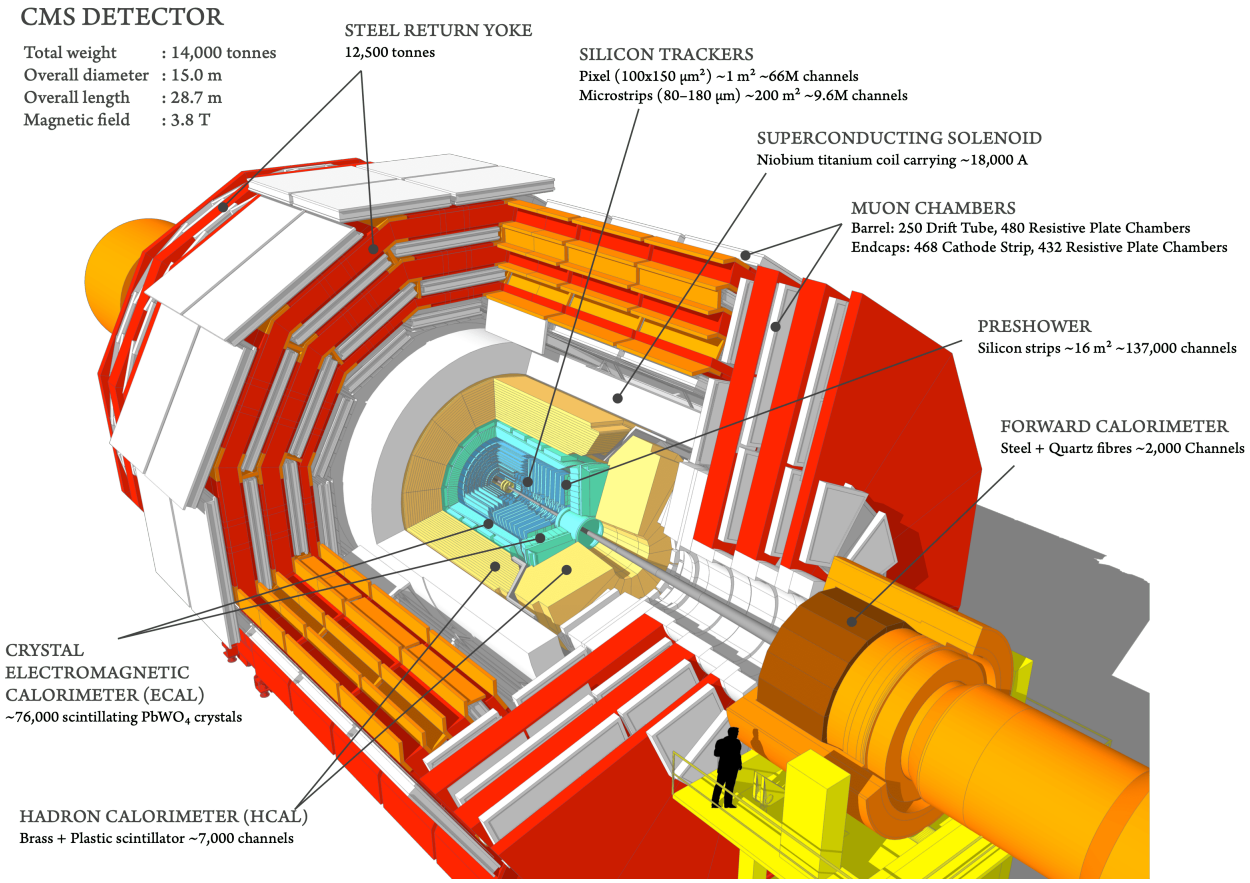

Figure 3.2: Cutaway diagram of CMS detector. *Source:* [32]

Inside the detector, the beams come from two opposite sides, and the collision occurs at the geometric center of the whole apparatus. Layers of different sensors surround the collision point. The different sub-detectors will be discussed in the next section.

3.2.1 Working of the CMS detector

In the CMS detector [33], a particle can be studied by:

- observing the particle's track,

- allowing it to be deposited on a surface, and then study its properties (charge, energy, etc.),
- and at times, a combination of observations of both methods.

Tracking detectors are employed to observe particles' tracks, calorimeters for the energy measurements of the particles, and muon chambers to identify muons. These detectors are arranged in layers around the collision point like an onion as depicted in the figure 3.3.

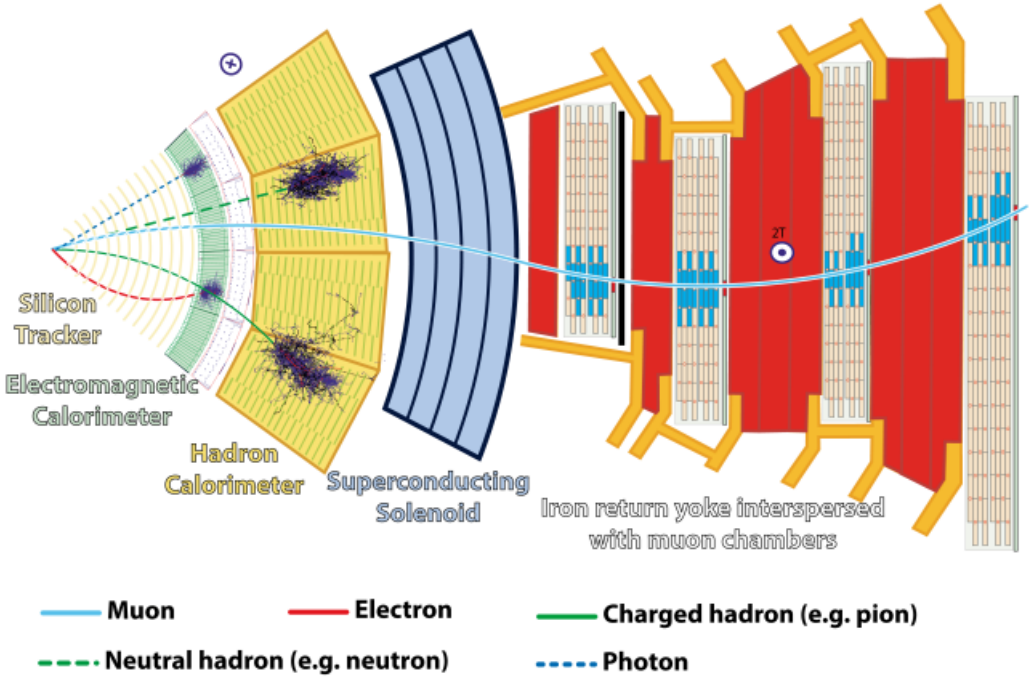

Figure 3.3: A slice of the CMS detector. *Source:* [34]

Various kinds of particles will be sensed by different sub-detectors and hence, identified. For instance, both the electrons and the photons will be detected by the Electromagnetic Calorimeter. However, since the tracker can track charged particles, the particle will be distinguished and identified based on the particle tracks. Hadron Calorimeters detect all kinds of hadrons (protons, neutrons, pions, etc.). Muon identification and energy measurements take place in the muon chambers. All sub-detectors have two parts - barrel and endcaps. The barrel is the region surrounding the collision point except for the beamlines, whereas the endcaps are along the beam pipe to record the collision information along with those directions. Let's understand each detector in detail:

Inner Silicon Tracker

As the name suggests, it tracks the charged particles and measures their momenta from the curve of their trajectories. It is wholly made up of silicon and is divided into pixels and strips. These pixels are susceptible to the passage of charged particles. A pixel lights up on getting hit by a charged particle. Observing all the lit pixels gives the particle's

path. There are three stacks of pixel detectors and about ten to eleven layers of strip detectors. The whole sensor has 75 million read-out channels meaning 75 million pixels or strips. What makes the tracker stand out as an excellent detector is its frequency of capturing particles' tracks from an event during a collision. The tracks are also used to identify the vertices where the particles are originated.

Electromagnetic Calorimeter (ECAL)

After the trackers, a layer of electromagnetic calorimeters captures and measures the energies and momenta of electrons and photons. This detector is made up of about 80,000 Lead-Tungstate ($PbWO_4$) crystals. In contrary to the heat calorimeters, these detectors measure the energy transferred by the electrons and photons. They do so by stopping the passage of all electrons produced during the collisions, using the $PbWO_4$ crystals. Electrons lose energy in the crystal, emitting photons by bremsstrahlung. These photons then generate a pair of an electron and a positron. These newly generated electrons and positrons will also produce photons, and the chain reaction will continue leading to a cascade of particles. This process is called an '**Electromagnetic shower**.' The total amount of secondary particles produced is proportional to the energy of the first incoming electron deposited on the calorimeter. A scintillator ($PbWO_4$ crystals here) is used to count the numbers of secondary particles. Photodiodes are appended at the tip of the crystals and measure the amount of scintillator light, which turns out to be directly proportional to the number of secondary particles produced, and this is proportional to the energy of the incoming electron. ECAL has an exceptional energy resolution [35] for electrons (estimated from Z boson decays) greater than 2 % in the central region of the ECAL barrel and is $2-5$ % elsewhere. For photons (estimated from Higgs boson decays), it ranges across the barrel from 1.1 % to 2.6 % and 2.2 % to 5 % in the endcaps.

Hadron Calorimeter (HCAL)

After the ECAL, there's a layer of Hadron calorimeter. As the name suggests, HCAL measures the energy of all the hadrons - protons, neutrons, pions, kaons, etc. Here the working principle of the calorimeter is quite similar to that of ECAL except that the dynamics of the shower produced by the incoming particles are complex. This complexity is due to the nuclear interactions. Also, some of the particles produced are neutral, and thus, it becomes difficult to detect their interactions. HCAL has an assembling detector made up of very dense brass absorber material capable of stopping the passage of hadrons. The brass layers have a layer of scintillator between them. HCAL is used efficiently in jets measurement.

The muon detection system

After we go past the solenoid, only the muons are left to be detected. For muons, we measure their trajectories from which we can estimate their momenta. The muon system is made up of drift tubes about 1 m long and 4 cm thick. The tubes are filled with the gas mixture, with anode wires in the middle. Thus, there is an electric field between the wires in the middle and the wires outside the tube. The gas mixture in the detector is chosen so that when a muon passes through it, the gas mixture gets ionized and, negative and positive ions drift in the magnetic field. At some point, the negative ions hit the anode, and a spike is observed, which confirms the passing of a muon through the tube. Using the tubes, we measure the drift time of the electrons produced by the passing muon. To estimate the correct direction of muons, a layer of drift tubes is used, making a brick-wall type structure.

The cathode strip chambers are used to measure the muon trajectories in the endcap region. These are gaseous detectors with layers of anode wires and cathode strips.

CMS Trigger system

At the time of Run 1, about 40 million collisions occurred per second (collision frequency - 40 MHz). On reading the information from the sub-detector, we get 1 MB of data for one collision. For 40 million collisions, we would get 40 TB of data per second which is beyond the data handling capability of any computer system. To cope up with this problem, we use a trigger system that works on reducing the data. The trigger is an online decision-making system that chooses only interesting collisions according to different criteria (e.g., transverse momentum of muons in the event). The trigger reduces the rate from 40 million collisions per second to 1000 collisions per second. Thus, 1 GB/s of data is comparably easy to handle for a computer system. The data collected by the trigger is then further analyzed. In CMS, there is a two-level trigger system: Level-1 Trigger and High-Level Trigger. More about trigger systems can be found in [36].

3.3 CMS Phase 1 Upgrades

Phase 1 upgrades [37] of the CMS detector aims at modifying the detector to perform at peak luminosity, $L_{peak} = 2.0 \times 10^{34}$ cm^{-2} s^{-1} with pile-up of ~ 50 and up to 300 fb^{-1} of integrated luminosity. As a part of the Phase 1 upgrades, the Hadron Calorimeter will be upgraded with new photodetectors and electronics during the Long shut down 2 (2019-21). The muon system is expected to be upgraded to increase the granularity output of the read-out channels by increasing the coverage area with more Cathode strip chambers (CSCs) and Resistive Plate Chambers (RPCs). The Trigger systems will be updated with new back-end electronics for improved bandwidth and processing capability. The

ultimate goal is to make the detector capable of tackling pile up to around ~ 60 and up to 300 fb^{-1} of integrated luminosity by the end of long shut down 2. The main Phase 1 upgrades are already done in Run 2 (in 2017), including installing a new pixel detector in 2016.

3.4 High Luminosity - LHC

Currently, at the LHC, a Higgs boson is produced once in around 10 billion collisions. To study the Higgs boson, its properties, or search various exotic phenomena associated with it, we need to have more and more Higgs bosons. We need to increase the number of collisions (integrated Luminosity) taking place in the collider.

The High Luminosity - LHC (HL - LHC) aims at the up-gradation of the present LHC. Figure 3.4 shows the evolution of LHC towards the HL - LHC [38]. Currently, we are at the long shutdown 2 (LS2) stage where many hardware in the experiments are being modified, and several engineering upgrades are being made.

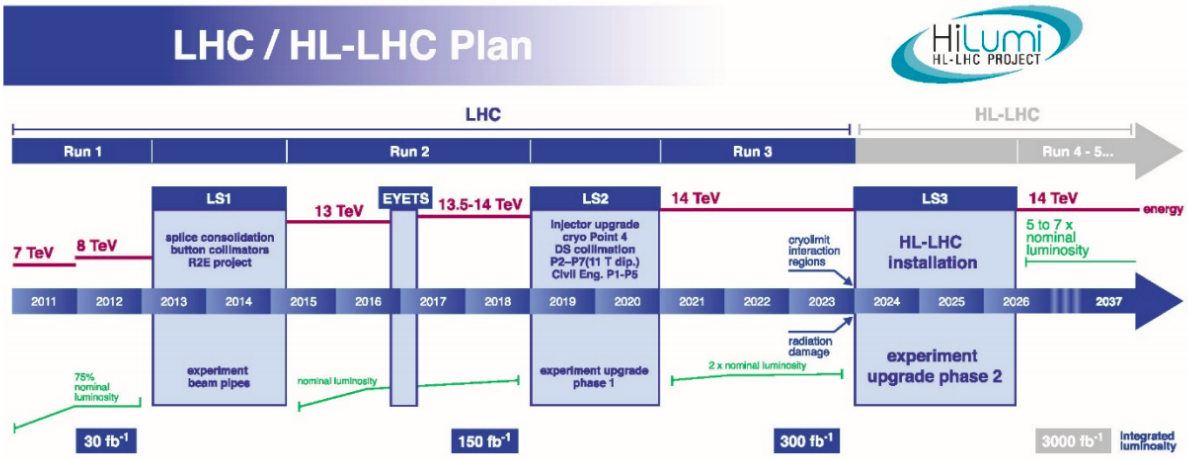

Figure 3.4: High Luminosity - LHC plan. *Source:* [38]

After Run 3, the LHC will undergo major upgrades to increase the luminosity by multiple folds. The main goal is to increase the peak luminosity to, $L_{peak} = 5 \times 10^{34}$ cm^{-2} s^{-1} with levelling and the integrated luminosity to 250 fb^{-1} per year, so as to achieve $L_{int} = 3000$ fb^{-1} at the end of twelve years after the HL - LHC installation. To increase the proton-proton collisions, the idea is to make the proton bunches denser at the collision point. This can be achieved using special magnets called inner triplets. These magnets will replace the existing ones at the interacting regions. Apart from this, many other sections of the accelerator will also be modified. It is estimated that more than 1.2 km of the LHC will be completely replaced by advanced instrumentation and hardware.

All the major upgrades at the LHC will also be accompanied by modifying the two general-purpose experiments - ATLAS and CMS.

3.5 CMS Phase 2 Upgrades

The CMS Phase II upgrade [39] aims to maintain the detector's good performance at HL - LHC luminosity. There are two significant reasons for the upgrades:

1. There will be an unprecedented number of events taking place. HL - LHC will ensure that an average of 200 proton-proton collisions per bunch crossing takes place. This is also called pile-up. High pile-up will pose a significant challenge for the detectors, and it won't be easy to mitigate the pile-up effects.

2. The rate of the data flow will be higher than ever. With increasing collision, there will be an increase in the radiation, and some detectors might not just survive such high radiation. Thus, some detectors will have to be replaced.

The tracker will be completely replaced during a Long shut down (LS3). The replacement tracker will be tolerant to high radiation and increased granularity. With this replacement, there will be extended coverage in the forward region. The Endcap region of both electromagnetic and hadronic calorimeters will be entirely replaced. For the muon system, new chambers will be installed in the forward region. Also, there will be an installation of totally new front-end electronics in drift tube chambers. Finally, the trigger systems will be upgraded with new back-end electronics. In a nutshell, all the sub-detectors will be upgraded, and their design will be improved for working at higher luminosities.

3.6 Event Reconstruction

The process of obtaining physical quantities from the raw data collected by the detector is called reconstruction [40]. Talking in terms of software processes, it is basically a method of reducing data where the principal target is analyzing and studying the data. During this procedure, collections of small units are used to provide a corresponding group of objects as outputs. This reconstruction procedure is done in three steps:

1. Object reconstruction within a sub-detector (Local reconstruction).

2. Global reconstruction in the whole detector.

3. Combing the above two levels to obtain final higher-level objects.

3.6.1 Local reconstruction

In the local reconstruction, RecHits[1] are produced that exhibit information about the position of particles and energy accumulations. Local reconstruction in the tracker occurs by using algorithms that search for the signals beyond some threshold values in the pixels. Combining the signals from adjacent pixels leads to clusters. In muon chambers, the drift time measurement and effective drift velocity are used to deduce the position of a muon in drift chambers. In the cathode strip chambers (CSCs), the arrival time of a muon is determined from induced charged distribution by the incoming muon. Local reconstruction in Electromagnetic calorimeters occurs by identifying the position, time of arrival, and energy of the electromagnetic energy accumulations. Reconstruction mechanism in Hadron Calorimeter is quite similar to ECAL, except that the reconstructed objects are quark jets or hadrons.

3.6.2 Global reconstruction

Global reconstruction employs a method where multiple objects recreated within different modules of a sub-detector during local reconstruction are combined to produce a combined physics object. This include:

- **Track reconstruction**

  It can be explained through five steps:

  1. Hit reconstruction: It is basically pixel clustering and approximation of position with irresolution.
  2. Whole track reconstruction using seed generation for the initial trajectory candidates.
  3. Plotting the trajectory.
  4. Resolving ambiguity.
  5. Fitting of the ultimate track.

  Uncertainties in track determination occur as a track might be reproduced using various seeds, or a typical seed may lead to multiple trajectories.

- **Vertex reconstruction**

  It is done in two steps:

  1. **Vertex finding**, in which the various tracks are clubbed together for vertex candidates. The algorithms for the same depends on the type of physics - primary vertex, secondary vertex, reconstruction of exclusive decays.

[1]RecHits: Reconstructed Hits in the calorimeters and trackers are often called **RecHits**.

2. **Vertex fitting**, in which various vertex parameters are estimated for given set of tracks. These parameters include position, covariance matrix, etc.

3.6.3 Combined reconstruction

In this level, the objects reconstructed in sub-detectors during the Global reconstruction phase are used as inputs for creating physics objects based on the whole detector.

- **Electron (e^-) and photon (γ) identification**

  Global Identification of e^- and γ is conducted through subsequent steps:

  1. First, the calorimeter data alone is used.
  2. In the next step, impacts in the pixel detectors in agreement with an e^- candidate are used. On comparing Electromagnetic Calorimeter clusters with the impacts in the pixel detector, if a match is found, the candidate is identified as an e^-; otherwise, the candidate is identified as a γ.
  3. Lastly, the electrons are selected based on the full track reconstruction sourced from the pixel impacts obtained during the previous step. Identification of photons is based on isolation cuts and exclusion of pions based on side shower shape and the reproduction of converted γ.

- **Muon identification**

  Recognition of muon is carried out using a combination of silicon tracker hits and final fitting of tracks. Isolation criteria are used to reject non-prompt muons from decays of mesons (B and D).

- **Jet reconstruction**

  This process involves reconstructing and identifying jets from the hadronization of scattered quarks and gluons. There are so many jet reconstruction algorithms. However, the majority of them use a clustering technique where calorimeter towers close to high E_T towers in terms of pseudorapidity (η) & azimuthal angle (ϕ) are summed together.

- **MET (missing E_T) reconstruction**

  The missing E_T is often a signature of new physics observed for many discovery/search channels. It is reconstructed by adding all the energy accumulations $\times \sin\theta$ for the whole calorimeter, furthermore considering transverse momenta of muons.

Chapter 4

Higgs Boson: Production and Decay & the H $\rightarrow \mu\bar{\mu}$ process

The Higgs boson is produced quite rarely in the pp collisions (once in 10 billion collisions). There are four main processes through which the Higgs boson can be produced [41]:

1. If a quark and anti-quark collide with each other by exchanging a virtual vector boson with each other, then a Higgs boson might be emitted. This process is called **Vector Boson Fusion**

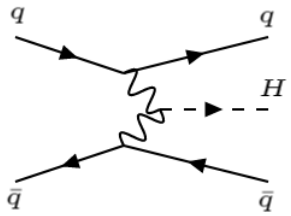

Figure 4.1: Feynman diagram of Vector Boson Fusion

2. There is a process in which a quark and anti-quark pair collide with each other, fusing into a vector boson. If this newly produced vector boson is of sufficient energy, it can emit a Higgs boson and a vector boson.

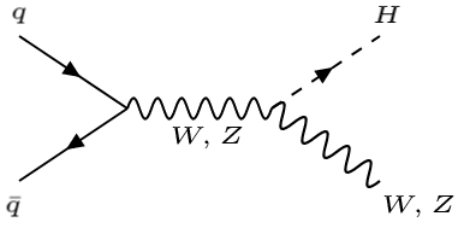

Figure 4.2: Feynman diagram of Higgs Strahlung

3. In particle colliders, if the colliding particles are either hadrons, then it is highly probable that the collision at the fundamental level is between two gluons that bind

the hadron. These gluons fuse to form a loop of virtual quarks. This production mode has a relatively much higher probability with respect to the vector boson fusion process and is called **Gluon fusion.**

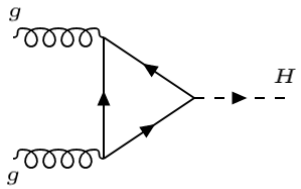

Figure 4.3: Feynman diagram of gluon fusion

4. **In association with a top quark(s)**: This is the production process with the smallest probability of all modes. In this process, two gluons fuse, decaying into a Higgs boson and a top anti-top quark pair.

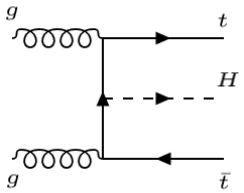

Figure 4.4: Feynman diagram of Higgs production in association with top quarks

4.1 Decay of Higgs boson

The Higgs particle has a very short mean lifetime of about 1.6×10^{-22} s. It's an extremely short-lived particle and decays almost instantly into a particle - anti-particle pair. Because of its interaction with most of the elementary particles, Higgs can decay through different channels [28]. All these channels have varied branching ratios.

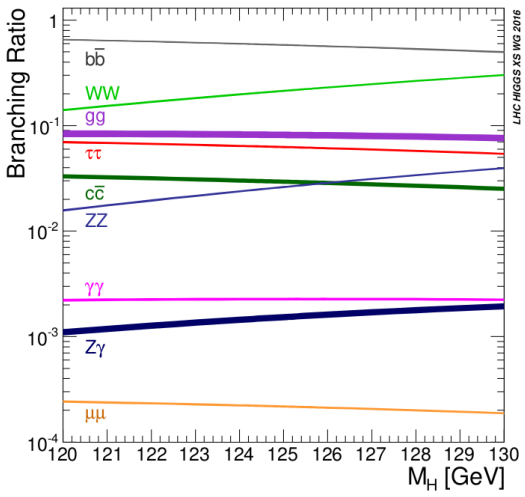

Figure 4.5: Branching ratios of various Higgs decay channels. *Source*: [28]

The branching ratio or fraction for a particular decay channel depends on the particles' masses, which the Higgs decays into. Some Higgs decay channels are discussed below:

1. **H** $\rightarrow \gamma\,\gamma$

   For the Higgs boson decaying into two photons, the branching ratio is 2.27×10^{-3}. Photons being massless make it difficult for their interactions with Higgs. Thus, Higgs decays into photons through a loop of virtual bosons or quarks.

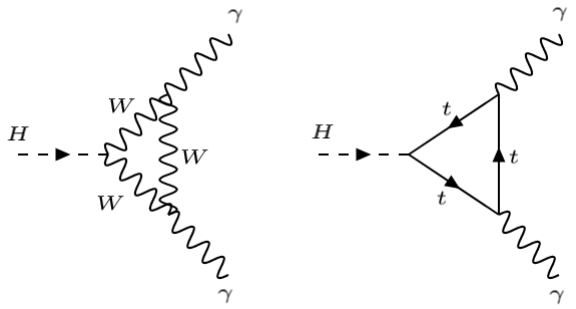

Figure 4.6: Feynman diagram of H $\rightarrow \gamma\,\gamma$ process

2. **H** $\rightarrow \tau\,\bar{\tau}$

   Tau (τ) pertains to the third generation of leptons and is the heaviest lepton. It is short-lived and thus decays before being detected. It can decay in three ways:

   - $\tau \rightarrow e^- + \nu_\tau + \bar{\nu_e}$
   - $\tau \rightarrow \mu^- + \nu_\tau + \bar{\nu_\mu}$
   - Hadronically

   Hadronic decays of tau result in charged hadrons or sometimes neutral pions as well. The branching ratio of the $H \rightarrow \tau\bar{\tau}$ is 6.27×10^{-2}. Study of this decay channel will deepen our understanding of the mechanism through which the Higgs interacts with the fermion sector.

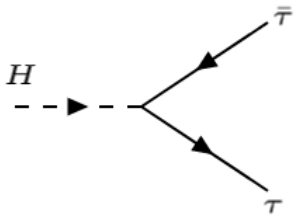

Figure 4.7: Feynman diagram of H $\rightarrow \tau\bar{\tau}$ process

3. **H** $\rightarrow ZZ$

   Z bosons produced by the decay of Higgs can further decay into a lepton anti-lepton pair such as e^-e^+, $\mu^-\mu^+$. The branching ratio of this decay mode is 2.62×10^{-2}.

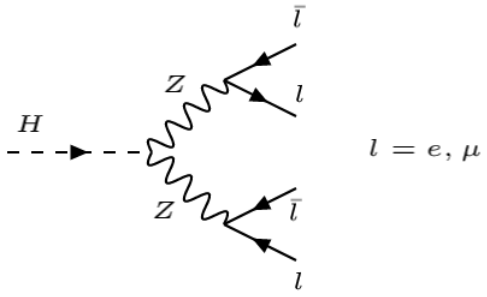

Figure 4.8: Feynman diagram of H $\rightarrow$ ZZ process

4. **H** $\rightarrow$ $b\bar{b}$

   Of all the decay modes, the branching ratio of the $H \rightarrow b\bar{b}$ is the highest (0.582). However, many other processes result in a pair of bottom quarks as the end products contributing to the extensive background. Hence, it is tough to observe this process.

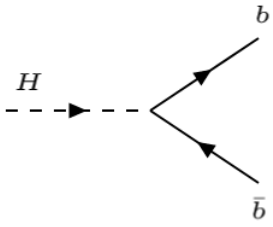

Figure 4.9: Feynman diagram of H $\rightarrow$ $b\bar{b}$ process

5. **H** $\rightarrow$ W^+W^-

   Like other massive elementary particles, W bosons to are unstable particles. Decay of Higgs produces a pair of W bosons with opposite charge. The newly produced W bosons can undergo both hadronic or leptonic decay. In hadronic decays, they decay into a quark anti-quark pair. Whereas in leptonic decays, they disintegrate into a lepton and its corresponding anti-neutrinos.

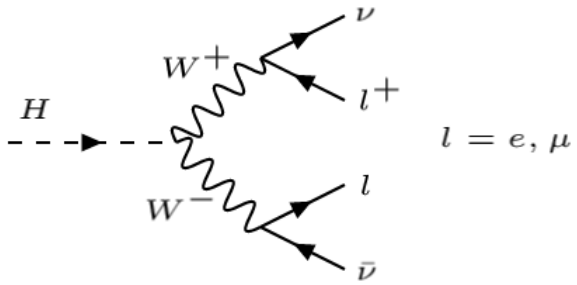

Figure 4.10: Feynman diagram of H $\rightarrow$ W^+W^- process

6. **H** $\rightarrow$ $\mu\bar{\mu}$

   Of all the decay modes, the process with the lowest branching ratio of 2.18×10^{-4} is that of $H \rightarrow \mu\bar{\mu}$.

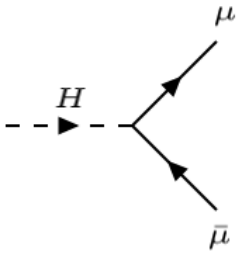

Figure 4.11: Feynman diagram of H $\rightarrow \mu\bar{\mu}$ process

We know that the Higgs boson gives mass to all other particles. However, we don't understand why does it give different masses to different particles? One way to answer this question is to study the interaction of Higgs with other particles - by **studying the decay of Higgs into other fundamental particles!**

4.2 The H $\rightarrow \mu\bar{\mu}$ process

The Higgs boson is known to have decay easily into heavier fundamental particles like $W^{\pm}$ bosons Z bosons, top quarks, and bottom quarks. However, its decay into lighter particles like muons is quite rare and very difficult to observe. If we look at figure 4.5 then, the H $\rightarrow \mu\bar{\mu}$ decay has the lowest branching ratio of all processes. Of all the Higgs bosons produced at the LHC, about one in 5000 Higgs decays into a muon anti-muon pair. The lower probability of the H $\rightarrow \mu\bar{\mu}$ process makes it interesting to study in future analyses.

As we saw in section 2.1.2, the fermions' masses depend upon the strength of their interaction with Higgs. Now each of the Yukawa couplings is a free parameter of the Standard Model, and hence, it should be tested experimentally. In recent years, the Higgs boson coupling to the third generation of quarks and leptons has been tested experimentally and firmly established. It is pretty consistent with the Standard Model predictions. The next step remains to probe the Higgs coupling to the second generation fermions, especially the lepton sector - 'μ.' This will be an excellent way to study the Higgs-fermion interaction at an unprecedented mass scale. Thus, studying the H $\rightarrow \mu\bar{\mu}$ process is essential for this reason.

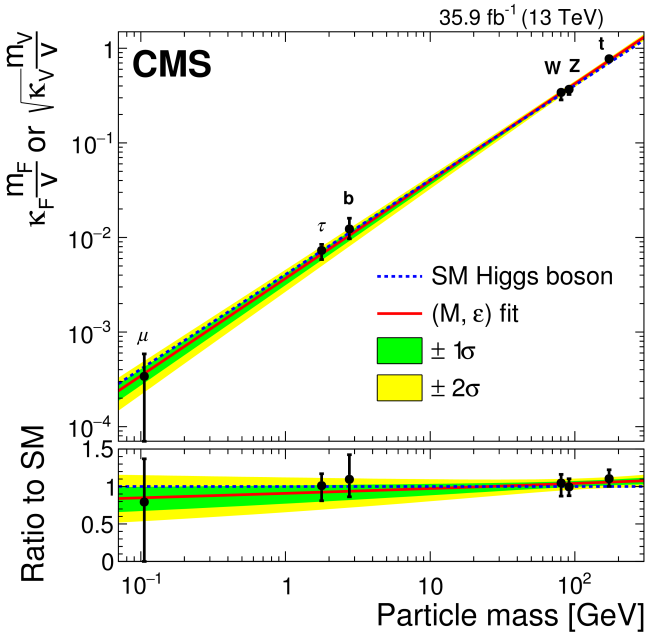

Figure 4.12: Standard Model Higgs couplings with different particles. *Source*: [42]

In figure 4.12, there are the measured coupling of particles of different mass with Higgs. There is uncertainty in the Higgs coupling with muons. Further studies of the H $\rightarrow$ $\mu\bar{\mu}$ process at higher luminosities will result in a more accurate measurement of the strength of this coupling. It is expected that deviation from the Standard Model predictions will be minor. However, if this deviation from the SM predictions persists, it **might** reveal New Physics beyond the Standard Model.

4.2.1 Recent developments

In a recent paper titled "Evidence for Higgs boson decay to a pair of muons" [43] published by the CMS collaboration in January 2021, results of H $\rightarrow$ $\mu\bar{\mu}$ analysis was presented. The pp collisions recorded at $\sqrt{s} = 13$ TeV at an integrated Luminosity of 137 fb^{-1} were analyzed. The process was observed with a significance of 3.0 σ compared to the expected 2.5. The data included a search for this process in which the Higgs was created by all four production mechanisms. When combined with the Run 1 data, this result raised both the anticipated and measured standard deviations by 1%. The best fit (μ) was $1.19^{+0.40}_{-0.39}$ (statistical uncertainty)$^{+0.15}_{-0.14}$ (systematic uncertainty).

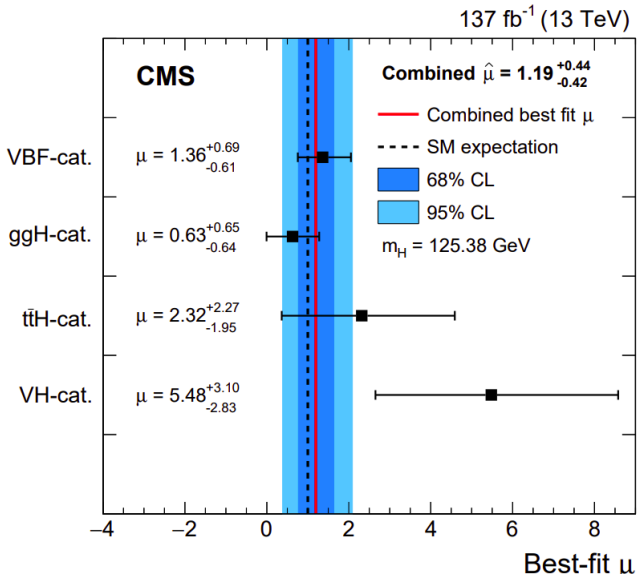

Figure 4.13: Best fit (μ) measured for $m_H = 125.38$ GeV for all four production categories. *Source*: [43]

As seen in figure 4.13, the processes in which the Higgs is produced via VBF and ggH modes are more sensitive.

In another paper titled "Sensitivity projections for Higgs boson properties measurements at the HL-LHC" [44] by the CMS Collaboration in the year 2018, sensitivity projections of various analyses were extrapolated to HL - LHC integrated luminosity (3000 fb^{-1}) using the Run 2 data which was recorded at $\sqrt{s} = 13$ TeV at 35.9 fb^{-1}. For the H $\rightarrow \mu\bar{\mu}$ process, two of the four Higgs production modes - gluon fusion and vector boson fusion, were taken into consideration. The paper presented the uncertainty projections for Run 2 (with systematic uncertainties) as well as for Yellow report[1] 2018 studies (with systematic uncertainties):

Scenario	L_{int} = 300 fb^{-1}		L_{int} = 3000 fb^{-1}	
	Statistical	**Total**	**Statistical**	**Total**
Run 2 (With systematic uncertainties)	42.0	43.0	9.1	13.0
YR18 (With systematic uncertainties)	42.0	43.0	9.1	9.6

Table 4.1: Expected $\pm 1\sigma$ uncertainties (in %) for the H $\rightarrow \mu\bar{\mu}$ channel. *Source*: [44]

As per Table 4.1, it is quite clear that at higher luminosities, there will be significant reduction in total uncertainties.

[1]CERN Yellow reports are a medium for communicating some work done at CERN, which are considered inappropriate for a publication in any journal.

Chapter 5

Research objective and methodology

In this chapter, the objective of the research is discussed. Also, the analysis methodology and techniques are explained.

5.1 Objective

The research aimed to extrapolate the sensitivity projections for the H $\rightarrow \mu\bar{\mu}$ process to Run 3 (Phase 1) luminosity and to HL - LHC (Phase 2) luminosity. The expected Phase 1 and Phase 2 integrated luminosities are $L_{int} = 300$ fb^{-1} and $L_{int} = 3000$ fb^{-1} respectively. As we observed in sub-section 4.2.1, the Vector Boson Fusion (VBF) production mode is the most sensitive of all; we analyzed the H $\rightarrow \mu\bar{\mu}$ process in which the Higgs is produced through this channel. For this, we used various Monte-Carlo samples corresponding to different signal and background processes. The analysis workflow was as follows:

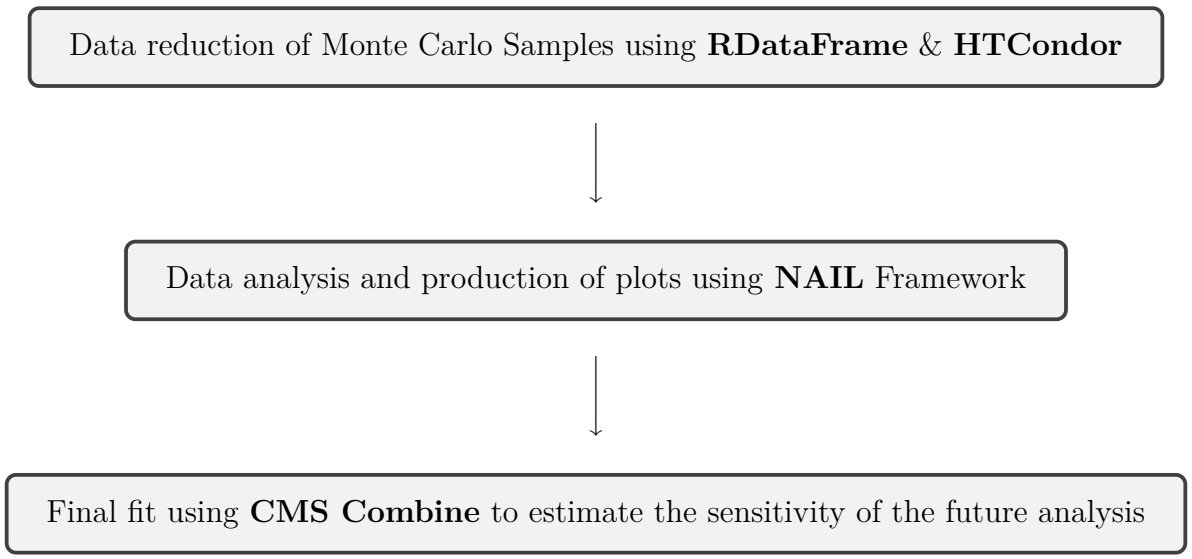

Each step in the analysis will be discussed in subsequent sections.

5.2 Data reduction using RDataFrame & HTCondor

The Monte Carlo data to be analyzed is vast, and it becomes necessary to reduce the data by employing some screening mechanism.

Skimming is the process of filtering the events with a loose pre-selection. We also compute some new variables based on the available data during this process. For skimming, a new tool of ROOT package [45] RDataFrame, was used.

5.2.1 ROOT's RDataFrame

The ROOT is a C++ based data analysis framework designed at CERN. It is an established scientific software tool kit. It is loaded with various components for the following tasks:

- big data processing,
- statistical analysis,
- data visualization and its storage.

One of the ROOT features is that it is blended very well with other computer languages (R, Python, etc.), making it flexible and easy to use for data analysis where functions and classes are imported from other languages. Of various ROOT's new classes, RDataFrame has emerged to be one of the most potent recent tools capable of handling multiple types of data files in a very efficient manner. Whatever type be the data source, it makes it very easy to filter and manipulate it to obtain desired outputs.

In our research, we used RDataFrame to filter the events as per the expected performances of the software and hardware resources at the end of Phase 1 and Phase 2 upgrades. RDataFrame made this task a lot easier than what it would take in other methods.

5.2.2 High Throughput Computing & HTCondor

Dealing with enormous amounts of data using a standard personal computer with limited computational power is almost impossible. Some operations may require computation time of more than half a day and the usage of many CPUs. This is where High Throughput computing [46] comes into the picture.

High Throughput Computing (HTC) is a robust model that allows the user to perform a huge amount of computational tasks that can be performed independently at the same time. An essential requirement of HTC is efficacious supervision of CPU cores, network traffic, memory, disk, and I/O. Note that both High-Performance Computing (HPC) and

High Throughput Computing (HTC) are different from each other.

In HPC, the ultimate goal is to increase the speed execution speed of a program as much as possible to obtain the output quickly. Whereas in HTC, there's no such requirement, and instead, the duplicate copies of a program with different input data are executed concurrently to obtain different outputs. These multiple program copies are called 'jobs.' HPC employs very high computational power for shorter periods and deals in floating-point operations per second. In contrast, HTC uses high computational power for more extended periods and deals in floating-point operations per year.

HTCondor

Condor [47] is a High Throughput Computing setting that can handle extensive sets of distributively owned workstations. It is an open-source software meant for the disseminated parallelization of computationally intense jobs. Developed by the University of Wisconsin–Madison, it can execute both sequential and parallel jobs. Thus, it is used by organizations such as NASA, CERN, etc.

For the research, multiple jobs were submitted on HTCondor in order to carry out the task of skimming efficiently at high speed. The complete code for skimming and submitting jobs on HTCondor used for the research is linked in Appendix B.

5.2.3 Information about the samples used

The Monte Carlo Samples used for the analysis were:

Process	**Monte Carlo Sample Name**
Higgs production by VBF	vbfHmm_2026POWPY
Higgs production by Gluon fusion	ggHmm_2026POWPY
Drell-Yan processes with 2 jets and $m_{jj} \sim 100$	DY100J2_2026MGPY
Drell-Yan processes with 1 jet and $m_{jj} \sim 100$	DY100J01_2026MGPY
Processes involving Top quarks	TT_2026POWPY
Electroweak processes with $Z \rightarrow 2$ leptons	EWKZ2JetsZToLL_2026MGPY

Table 5.1: Processes and corresponding Monte Carlo samples used in the analysis

The generators used for production of the Monte Carlo samples are abbreviated as follows:
POW: Herwig
PY: Pythia
MG: MadGraph

5.3 Data analysis and production of plots using NAIL

Natural Analysis Implementation Language (NAIL) is a primarily python-based framework developed at the University of Pisa and INFN Pisa. It allows the user to communicate the event processing operations declaratively, eliminating the need for an event loop and explicit loops on sets of objects. NAIL has ROOT's RDataFrame (see 5.2.1) as a backend.

It is aimed at following:

- development of the analysis,
- querying for intermediate results,
- updating the event processing strategy,
- adding systematics or exploring optimizations.

The final aim is not only to define the "event processing" in a declarative way, but the complete analysis, including building signal/background prototypes from a set of histograms and determining the statistical interpretation. NAIL allows us to visualize the analyzed data as well as obtain data cards for different fitting purposes.

The NAIL code on Github used for the research is linked in Appendix B.

5.4 Final fitting using CMS Combine

Data Cards are used for fitting histograms. They contain information about systematics, processes, background, etc.

The Combine [48] is a command-line tool configured with "data cards" for performing many standard statistical calculations. The tool makes use of RooFit and RooStats. Combine stores all information about the fit in '.root' files.

5.4.1 Plots of the original analysis

The CMS paper on $H \to \mu\bar{\mu}$ process [43] included results of searches for this process through all four production modes (VBF, ggH, $t\bar{t}H$ and VH). For the VBF mode, the observed and predicted distributions of the Deep Neural Networks (DNN) discriminants are shown in Figure 5.1, 5.2 and 5.3.

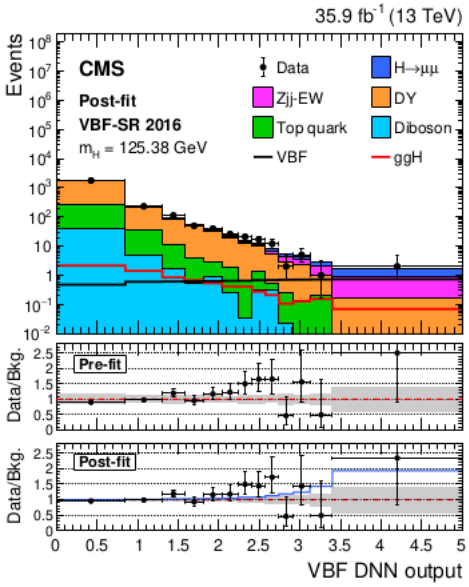

Figure 5.1: DNN Distribution in the VBF region for 2016 collision data at 35.9 fb^{-1}.
Source: [43]

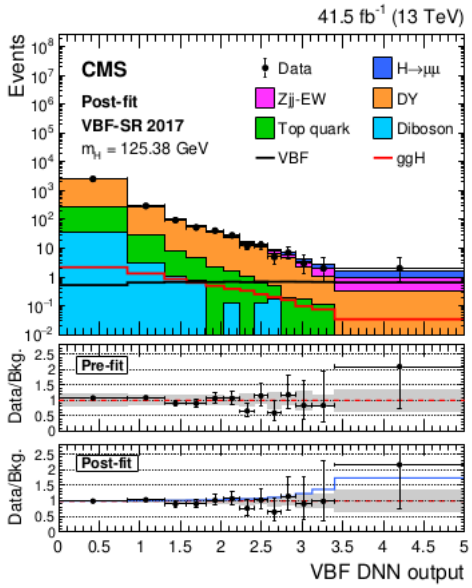

Figure 5.2: DNN Distribution in the VBF region for 2017 collision data at 41.5 fb^{-1}.
Source: [43]

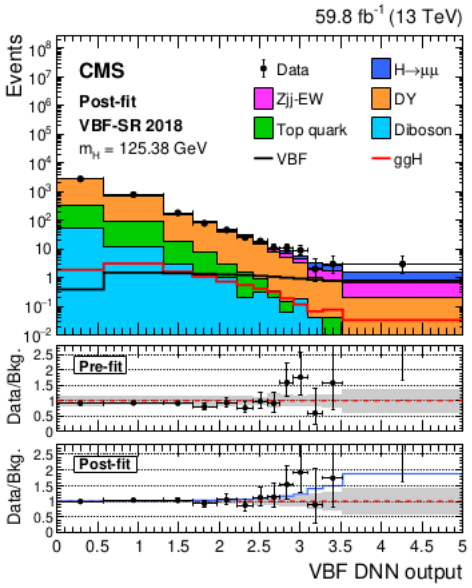

Figure 5.3: DNN Distribution in the VBF region for 2018 collision data at 59.8 fb^{-1}. *Source*: [43]

Figures 5.1, 5.2 and 5.3 correspond to the output DNN distributions of the VBF production mode for data collected in three consecutive years (2016, 2017, and 2018) compared with the post-fit background estimates for the contributing SM processes.

5.4.2 Obtaining yields and scaling the original analysis

In our research, first, the yields of the normalized histograms from the data card of the original analysis were obtained. The PyROOT code on Github used for the same is linked in Appendix B.

A similar PyROOT code was used for calculating the total yields of the normalized histograms of Phase 1 and Phase 2 MC samples using the data card obtained using a Python code.

Later, the ratios of Phase 1 and Phase 2 yields to the original analysis were calculated. The yields of the original histogram were then multiplied by the ratios of the yields obtained before. The original analysis (signal + background) was scaled to expected Phase 1 and Phase 2 cuts at different integrated luminosities. Using Combine, the significances (standard deviations) and uncertainties (fit diagnostics) were determined at various integrated luminosities. The total yields and final plots of the standard deviations and uncertainties are presented in Chapter 6.

Chapter 6

Results

In this chapter, all the results obtained at various stages of the research are presented, and subsequent inferences have been drawn.

6.1 Skimming of samples

The Monte Carlo samples used for the research had a considerable number of events (for both signal and background). It isn't easy to handle such a large amount of events as it requires too much computational power.

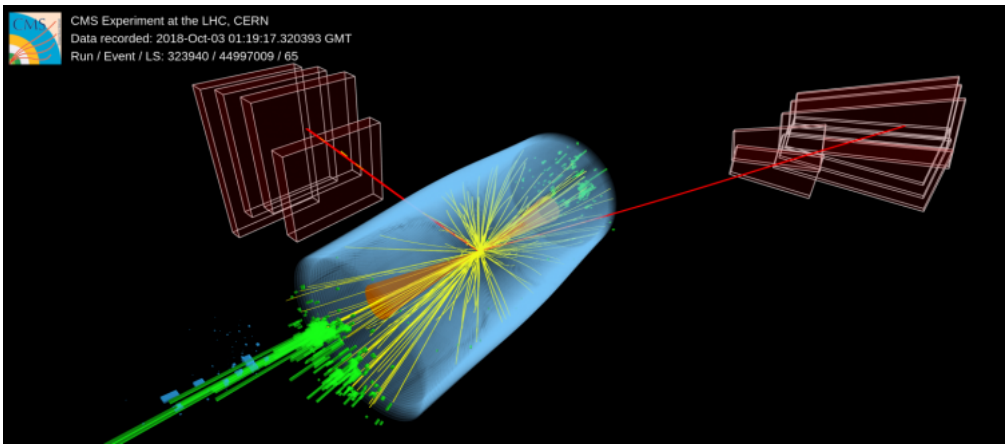

Figure 6.1: A candidate Higgs boson produced via vector-boson fusion (VBF) decays into a pair of muons (solid red lines), with an invariant mass of 125.01 GeV and per-event mass uncertainty of 1.83 GeV. The two forward VBF - jet candidates are depicted by the orange cones whose invariant mass (m_{jj}) is 2.19 TeV. *Source*: [49]

Figure 6.1 shows what a signal event looks like. Therefore we need to apply event selection to reduce the background and keeping a large fraction of the signal.

To tackle large amounts of data, a code for event selection was employed to screen events based on the following muon and jet definitions:

For Run 3 Analysis

- Muons:
  - ★ $|\eta| < 2.4$
  - ★ p_T 20 GeV
  - ★ $110 < \mathrm{M}_{\mu\mu} < 150$ GeV
- Jets (PUPPI[1] [50] jet for $|\eta| < 2.5$) :
  - ★ $|\eta| < 4.7$
  - ★ $p_T > 35, 25$ GeV
  - ★ $\mathrm{m}_{jj} > 400$ GeV
  - ★ $\Delta\eta_{jj} > 2.5$

For HL - LHC Analysis

- Muons:
  - ★ $|\eta| < 2.8$
  - ★ $p_T > 20$ GeV
  - ★ $110 < \mathrm{M}_{\mu\mu} < 150$ GeV
- Jets (PUPPI jet for $|\eta| < 4.0$):
  - ★ $|\eta| < 4.7$
  - ★ $p_T > 35, 25$ GeV
  - ★ $\mathrm{m}_{jj} > 400$ GeV
  - ★ $\Delta\eta_{jj} > 2.5$

The resultant number of events and size of the samples are summarized in the table 6.1

Monte Carlo Sample Name	**No. of events before Skimming**	**Sample size (GB) before Skimming**	**No. of events after Skimming**	**Sample size (MB) after Skimming**
vbfHmm_2026POWPY	7.11×10^5	60	1.14×10^5	99.5
ggHmm_2026POWPY	7.99×10^5	64	3.01×10^4	26.6
DY100J2_2026MGPY	1.95×10^7	1.6×10^3	4.01×10^4	33.4
DY100J01_2026MGPY				
TT_2026POWPY	2.69×10^8	2.3×10^4	3.86×10^4	42.3
EWKZ2JetsZToLL_2026MGPY	1.99×10^7	1.7×10^3	2.48×10^4	23.6
Total	**3.09** $\times 10^8$	**26.42** $\times 10^3$	**2.14** $\times 10^5$	**225.4**

Table 6.1: Summary of Monte Carlo samples' size and events before and after skimming

[1]**PileUp per particle Identification (PUPPI)**: It is an algorithm that is used to reduce the pile-up contamination from the jets.

A total of **26.42 TB** of data was screened. With the aforementioned selection cuts, the events were reduced from **3.09** $\times 10^8$ to **2.14** $\times 10^5$. The resultant $\sim$ 200 thousand events are easier to handle and can be used for further analysis. After skimming, the sizes of the samples were reduced to a few MBs.

6.2 Plots obtained using NAIL

As discussed in the section 5.3, the NAIL framework was used for the computation of variables, events filtering, making the final plots, and also the data card. The plots obtained using NAIL were as follows:

6.2.1 Plots of Phase 1 variables

For all the plots, Data/MC = 1, as we are using only simulations. The lower panel shows the '(Data/simulation) - 1', so it is equal to zero by definition. The plot show both the expected statistical uncertainty of data and the statistical uncertainty related to the limited size of the simulated events.

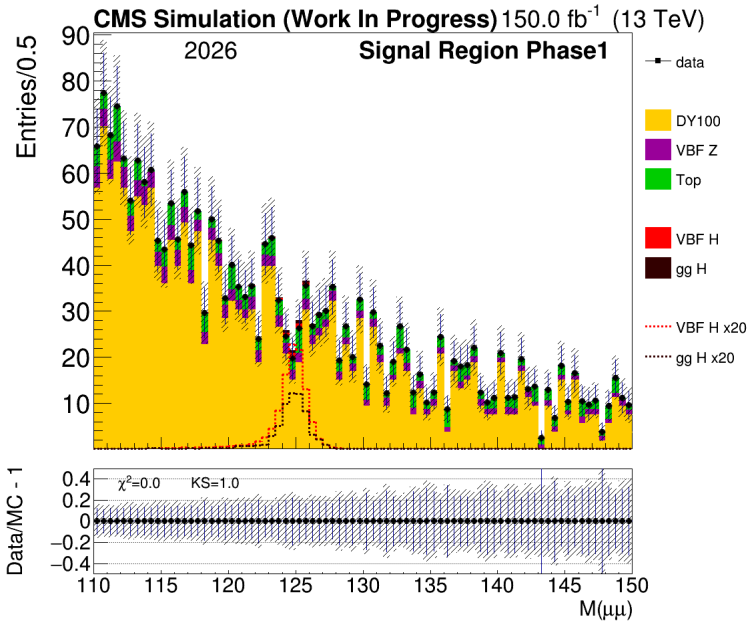

Figure 6.2: Di-muon Invariant mass

Figure 6.2 shows the distribution of invariant mass ($m_{\mu\mu}$). The dimuon mass peak at 125 GeV for the Higgs boson, while there is no peak for the other backgrounds.

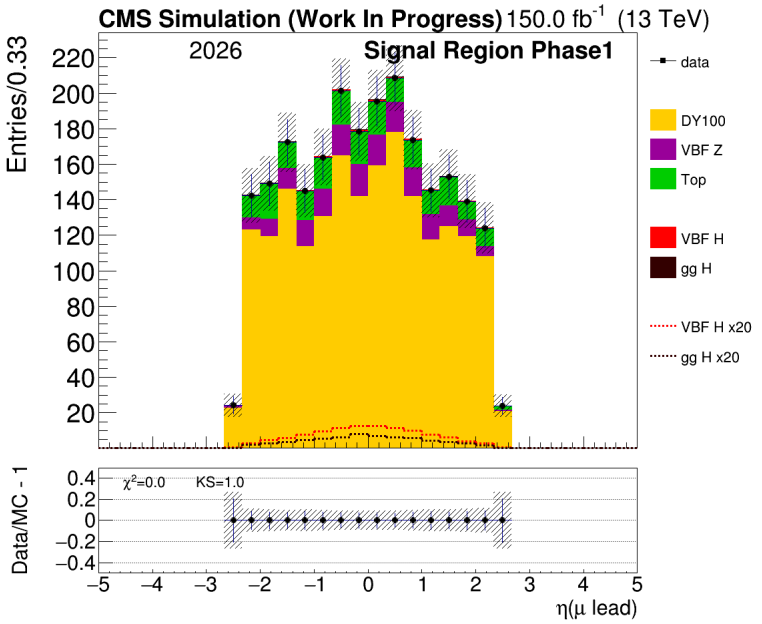

Figure 6.3: η of Leading muons

In figure 6.3, a distribution of the pseudorapidity (η) of the leading muons is plotted. The distribution is fairly symmetric about the origin. There are more leading muons with pseudorapidity in the range: -1 < η < 1 compared to other values.

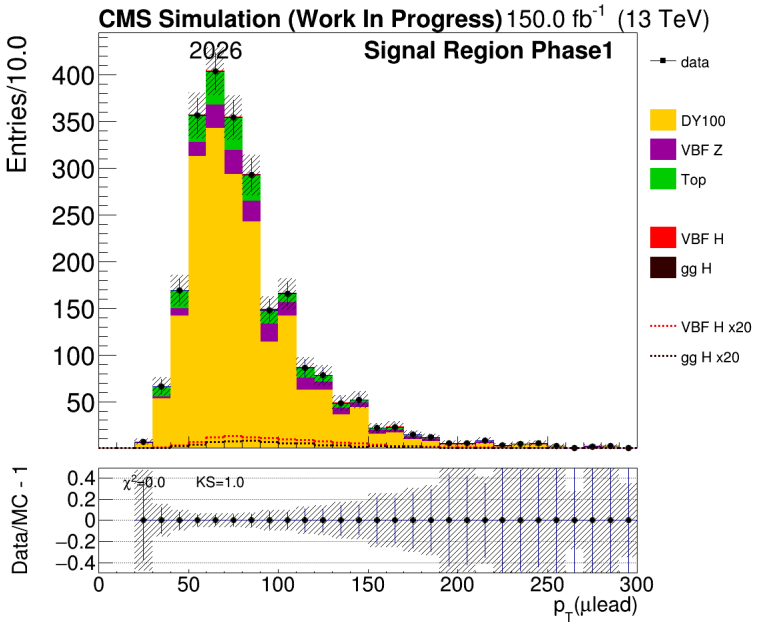

Figure 6.4: p_T of Leading muons

The above distribution of the transverse momenta of leading muons peaks in 60 - 70 GeV intervals. There are only a few leading muons with very high values of p_T.

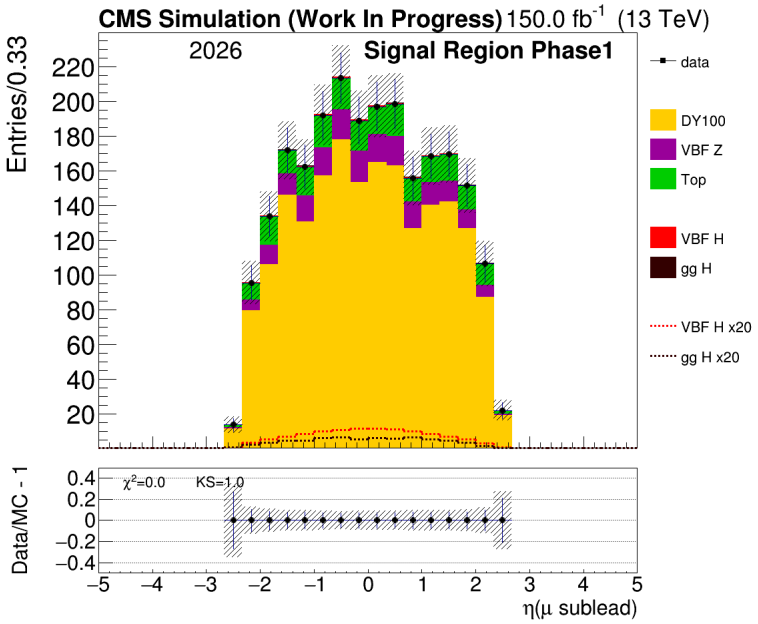

Figure 6.5: η of Sub-leading muons

Looking at figure 6.5, it can be said that the distribution of η for sub-leading muons is symmetric too. There is no substantial difference in the number of sub-leading muons with positive and negative values of pseudorapidity.

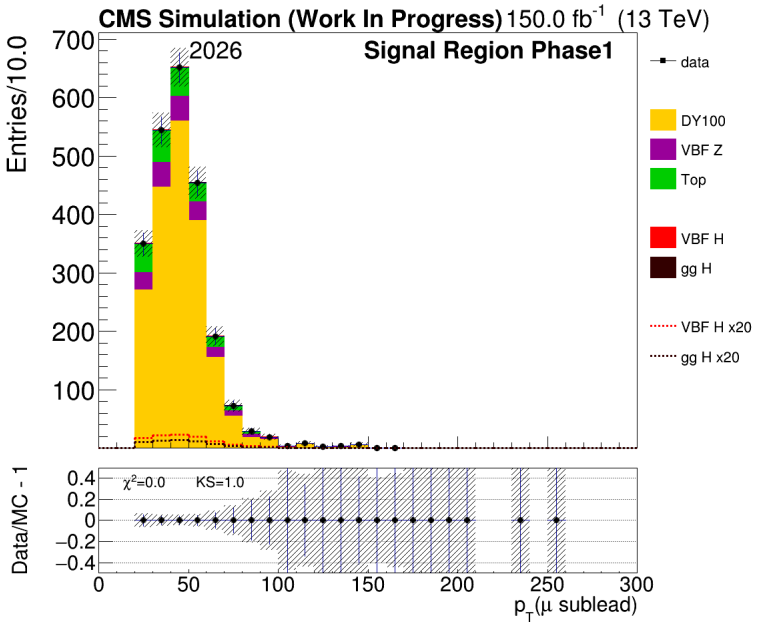

Figure 6.6: p_T of Sub-leading muons

The distribution of transverse momenta of sub-leading muons peaks in the interval of 40 - 50 GeV. There are very few sub-leading muons with values of p_T more than 100 GeV.

6.2.2 Plots of Phase 2 variables

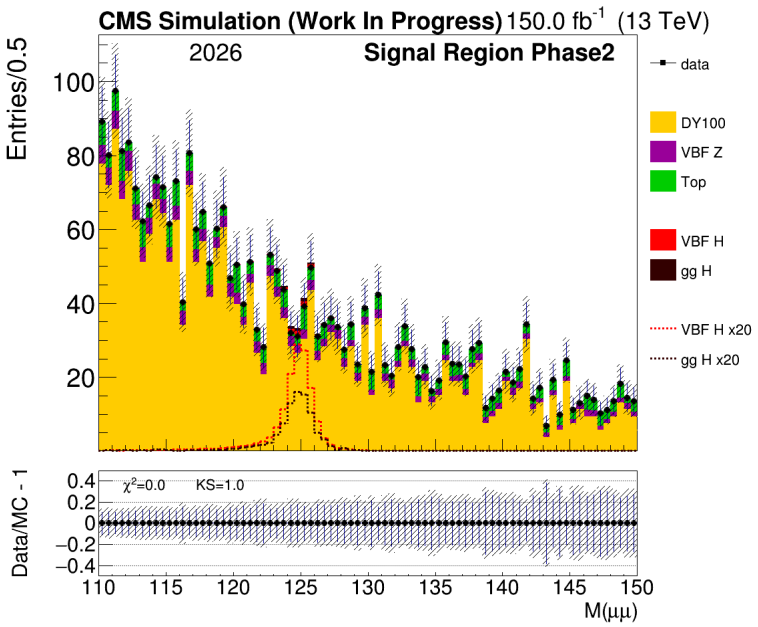

Figure 6.7: Di-muon Invariant mass

Like for Phase 1, the dimuon mass for Phase 2 also peaks at 125 GeV for the Higgs boson, while there is no peak for the other backgrounds.

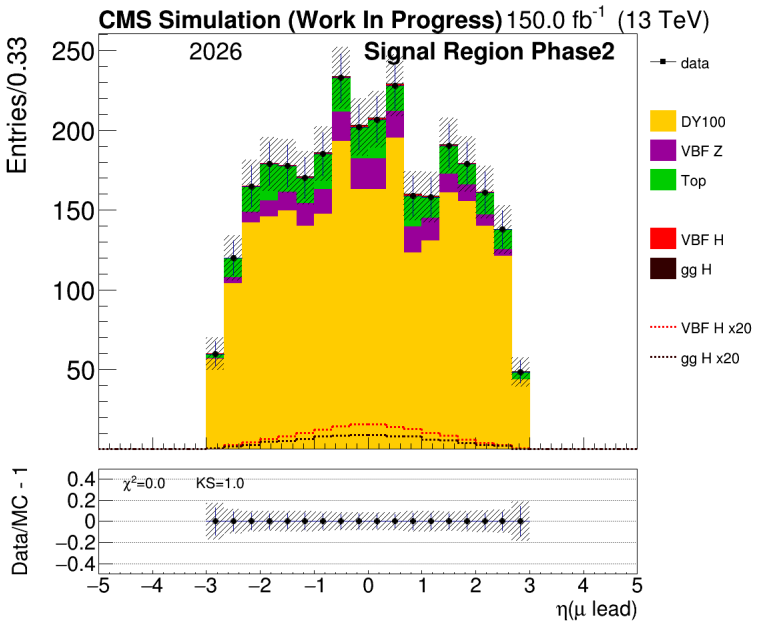

Figure 6.8: η of Leading muons

For Phase 2, the pseudorapidity distribution for the leading muons has two major peaks in the interval -1 $< \eta <$ 1. This distribution is also symmetric about the origin.

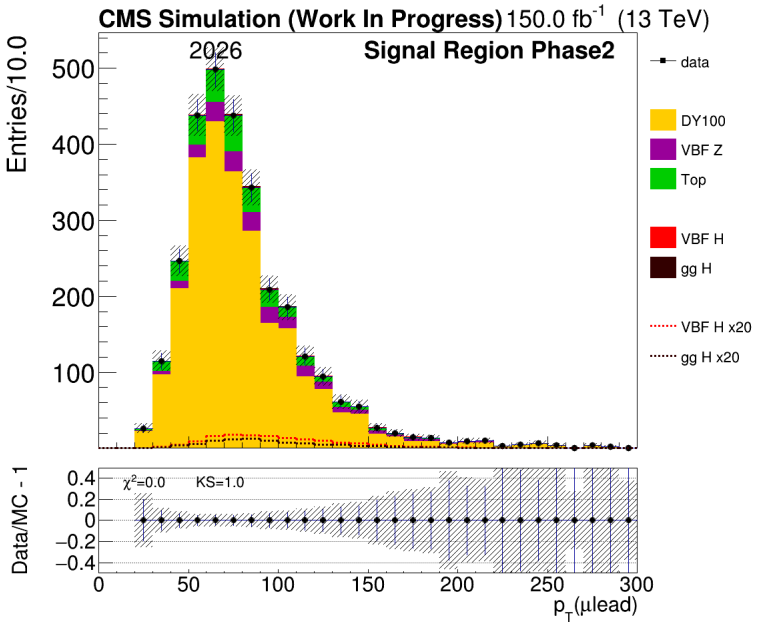

Figure 6.9: p_T of Leading muons

The distribution of transverse momenta leading muons in figure 6.9 has the peak in the interval 60 - 70 GeV. Very few leading muons have exceedingly high value of p_T.

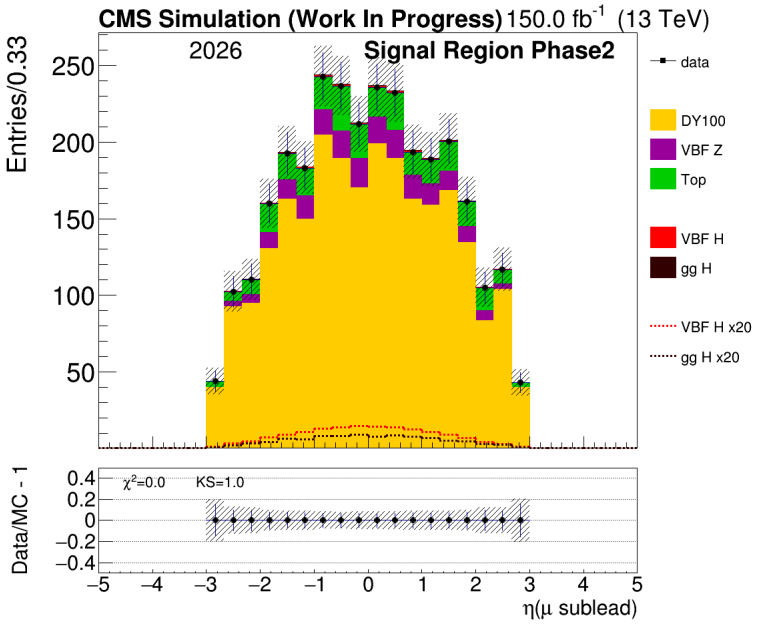

Figure 6.10: η of Sub-leading muons

For Phase 2 as well, the distribution of η for sub-leading muons is fairly symmetric.

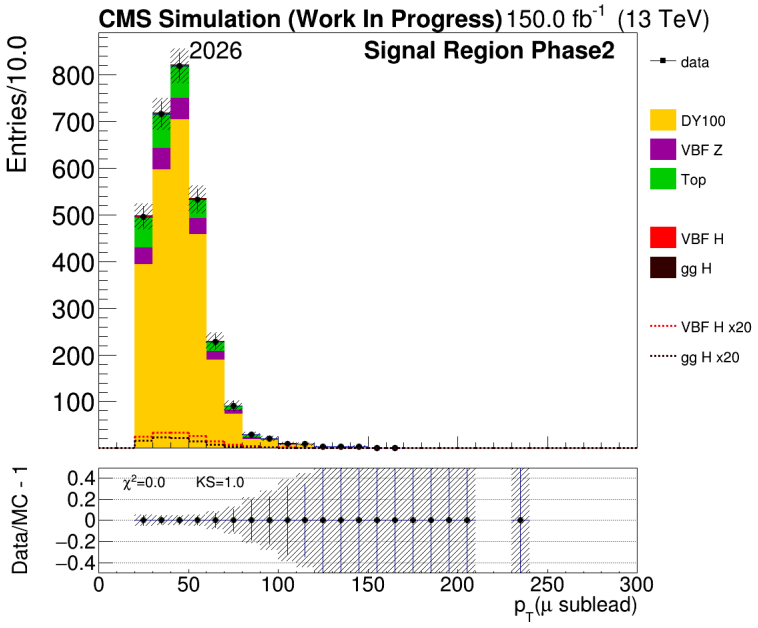

Figure 6.11: p_T of Sub-leading muons

The distribution of the transverse momenta of the sub-leading muons peaks in the interval 40 - 50 GeV.

6.3 Final fitting

The fit is performed using a likelihood ratio. All the systematic uncertainties are modeled using nuisance parameters with a probability distribution like a Gaussian, and they are included in the fit. In fitting, we use the yields of the different samples.

Sample / Process	**Total yields at L_{int}**		
	XX = **16** (35.9 fb^{-1})	**17** (41.5 fb^{-1})	**18** (59.8 fb^{-1})
vbfHmm_20XXPOWPYDIPOLE	7.1	7.5	11.9
ggHmm_20XXAMCPY	6.2	6.4	9.6
DYJ2_20XXAMCPY	1278.4	1524.8	2328.9
DYJ01_20XXAMCPY	782.2	985.5	1358.9
EWKZ105CORR_20XXMGHERWIG	74.0	78.7	127.1
Top	275.4	290.9	422.8

Table 6.2: Yields of the normalized samples (2016, 2017 & 2018) of the original analysis at various integrated luminosities

Sample / Process	**Total yields at L_{int} = 150 fb^{-1}**	
	Phase 1 Analysis	**Phase 2 Analysis**
vbfHmm_2026POWPY	5.6	7.6
ggHmm_2026POWPY	3.3	4.7
DY100J2_2026MGPY	1301.7	1701.4
DY100J01_2026MGPY	630.9	774.9
TT_2026POWPY	217.8	283.7
EWKZ2JetsZToLL_2026MGPY	187.7	200.0

Table 6.3: Yields of the normalized samples of the Phase 1 and Phase 2 analysis at L_{int} = 150 fb^{-1}.

Then we scale the data card, meaning the plot of the fit of the original H $\rightarrow \mu\bar{\mu}$ analysis. Then using the data card, **Significances** (Standard Deviations) and **Uncertainties** at various integrated luminosities are determined.

$\mathbf{L}_{int}$ (fb^{-1})	σ_{Phase1}	σ_{Phase2}
135	0.54	0.68
150	0.57	0.72
300	0.79	0.99
500	0.99	1.25
1000	1.36	1.71
2000	1.84	2.30
3000	2.18	2.72

Table 6.4: Significance of Phase 1 and Phase 2 analyses at various integrated luminosities

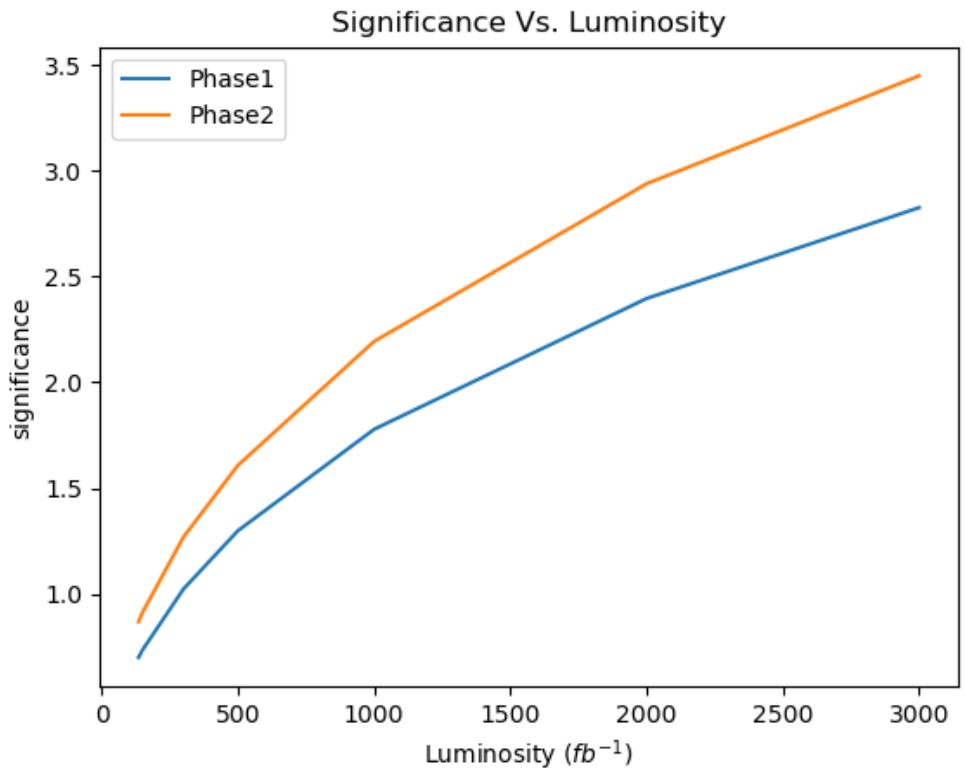

Figure 6.12: Plot of standard deviations of Phase 1 and Phase 2 fits at various integrated luminosities

Plot in figure 6.12 is of the p-value (standard Deviations) for the hypothesis that H$\rightarrow \mu\mu$ does not exists that is expected if the H$\rightarrow \mu\mu$ exists.

$\mathbf{L}_{int}$ ($\mathbf{fb}^{-1}$)	**Uncertainty (at 68% Confidence Level)**	
	Phase 1 analysis	**Phase 2 analysis**
135	2.06	1.64
150	1.95	1.56
300	1.40	1.12
500	1.10	0.88
1000	0.80	0.65
2000	0.60	0.49
3000	0.51	0.42

Table 6.5: Uncertainties in signal strength (at 68 % CL) of Phase 1 and Phase 2 fits at various integrated luminosities

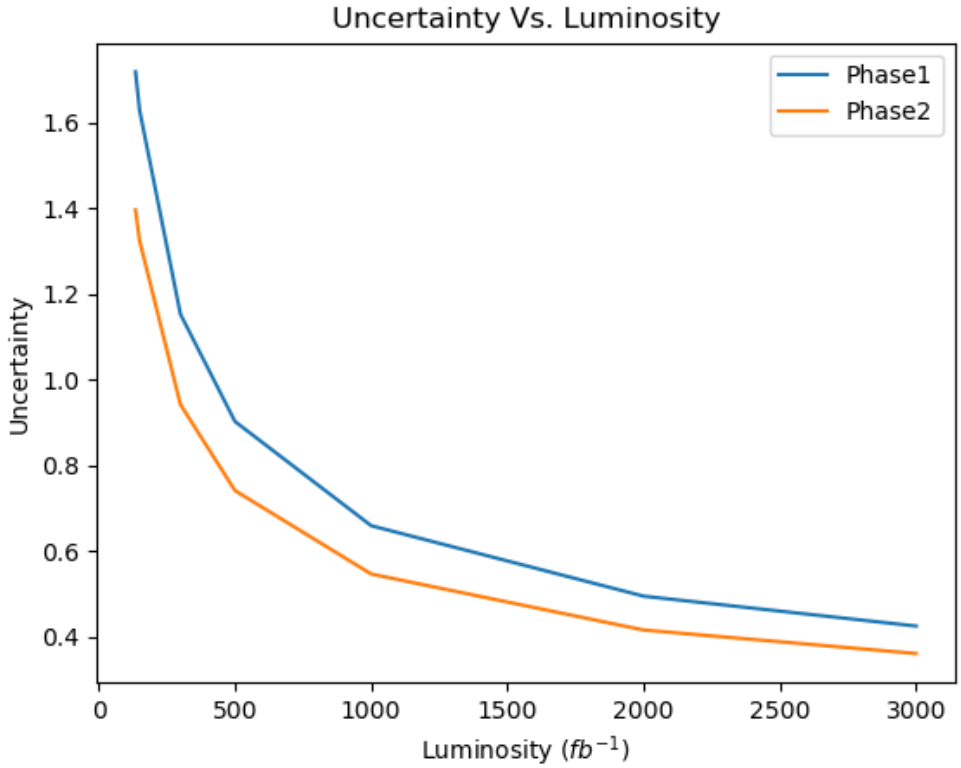

Figure 6.13: Plot of uncertainties (at 68 % CL) of Phase 1 and Phase 2 fits at various integrated luminosities

The plot in figure 6.13 is of the expected uncertainty on the signal strength for Phase 1 and Phase 2 analysis at various integrated luminosities.

Chapter 7

Conclusion and Future plans

7.1 Inferences

From the final results, we can make the following inferences:

- We can safely conclude that the analysis sensitivity will increase, i.e., the analysis will either **confirm** or **reject** the existence of the H$\rightarrow \mu\mu$ with increasing statistical power.
- From the final results, it is quite evident that with **increasing luminosity**, there will be **appreciable increase** in the significance and **decrease in uncertainties.**
- Larger muon acceptance (from 2.4 $\rightarrow$ 2.7) and the larger tracker acceptance (PUPPI η from 2.4 $\rightarrow$ 4.0) will result in the increase in the significance.
- If we look at the plot in figure 6.12 for Phase 2, 2σ is obtained at 1000 fb^{-1} instead of 3000 fb^{-1}; approximately five years earlier than anticipated.

To summarize, Phase 2 upgrades will have a remarkable positive impact on the studies of the H$\rightarrow \mu\mu$ process. Moreover, it will be exciting to study this process at higher luminosities.

7.2 Future plans

The project was undertaken as a part of the Snowmass studies of the rare decays of the Higgs boson. This project as a whole focuses on the comprehensive study and extrapolation of sensitivity projections for the H$\rightarrow \mu\mu$ process at higher luminosities.

The research carried out as a part of this dissertation was quite preliminary. For the H$\rightarrow \mu\mu$ process, only the Vector Boson Fusion (VBF) production mode was analyzed. A more complete study of the H$\rightarrow \mu\bar{\mu}$ will be obtained by combining the results of the other three channels:

- ggH production channel
- Higgs production in association with a vector gauge boson
- Higgs production with a top anti-top quark pair

A comprehensive study of this decay process will give a more profound idea about what we can expect from the Run 3 and HL - LHC operation.

Eventually, these studies need to be combined with the final Higgs searches. This will throw more light upon the study of the Higgs-muon coupling.

One of the significant limitations of the dissertation was the less number of available samples for analysis due to Covid - 19 pandemic. The inclusion of more latest Monte Carlo Samples will enable us to give more accurate sensitivity projections for this process.

Appendix A

Basic concepts and definitions

- **Cross section**
  In high energy physics, the probability of a particular process or reaction is quantified in terms of cross section (σ). Its dimensions are [M^0 L^2 T^0] and is expressed in barns (b).

$$1 \text{ b} = 10^{-28} \text{ m}^2$$

- **Luminosity**
  Luminosity ($\mathcal{L}$) can be thought of as a number that, when taken a simple product with the total cross section (σ) of a process, results in the total number (A) of collisions occurring per unit of time, i.e.,

$$A = \mathcal{L} \cdot \sigma$$

  Expressing the luminosity in terms of collider parameters, we get,

$$\mathcal{L} = \frac{n_x \, n_y \, N_x \, N_y \, f}{4\pi r^2}$$

  where

  n_x = No. of particles in a bunch revolving in the collider in one direction.
  n_y = No. of particles in a bunch revolving in the collider in opposite direction.
  N_x = No. of bunches of particles revolving in the collider in one direction.
  N_y = No. of bunches of particles revolving in the collider in opposite direction.
  f = frequency of circulation of beam in the collider.
  r = average transverse radius of a bunch.

  Luminosity is expressed in inverse barn per second (b^{-1} s^{-1}).

$$1 \text{ b}^{-1} \text{ s}^{-1} = 10^{28} \text{ m}^{-2}\text{s}^{-1}.$$

- **Integrated Luminosity**
  Integrated luminosity [51] can be expressed as:

$$\mathcal{L}_{int} = \int_0^t \mathcal{L}(t')dt'$$

  t = Total sensitive time.

- **Branching ratio**
  Decay modes can be described as the final states of the particle following its disintegration. The likelihood of a particle to decay through a specific decay mode is called the Branching ratio (BR) or branching fraction.

- **Signal strength (μ)**
  Best fit or signal strength is defined as

$$\text{Signal strength } (\mu) = \frac{\text{Measured cross section}}{\text{expected cross section (predicted by the standard Model)}}$$

  $\mu = 0$: No Higgs boson event.
  $\mu = 1$: Higgs boson as per the SM expectations.
  $\mu = 2$: 2× Higgs boson events, as per the Standard model predictions.

- **Transverse momentum (p_T)**
  Transverse momentum can be defined as the momentum (of particles or other objects) perpendicular to the direction of the beam axis.

$$p_T = \sqrt{p_x^2 + p_y^2}$$

  where p_x and p_y are momentum of particle along the axis.

- **Pseudorapidity (η)**
  It is an invariant quantity used instead of polar angle in particle collider experiments.

$$\eta = -ln\left[tan\frac{\theta}{2}\right]$$

  θ = Angle between the three-momenta and +ve side of the beam axis.

  Pseudorapidity is independent of the particle's mass or energy but is a function of the polar angle.

- **Azimuthal angle (ϕ)**
  It is determined as

$$\phi = \tan^{-1}\frac{p_y}{p_x}$$

.

- **Invariant mass (m_o)**
  According to the theory of special relativity, the Total energy (E) of a particle is related with its rest mass (m_o) and momentum (p) through the following equation

$$E^2 = p^2c^2 + m_0^2c^4$$

The rest mass of a particle can be derived from this relation

$$E^2 - p^2c^2 = m_0^2c^4$$

$$m_o^2 = \frac{E^2}{c^4} - \frac{p^2}{c^2}$$

Appendix B

Links to Github Repositories

- **Code for data reduction:**

  `https://github.com/mthakorecern/DelphesSkim/tree/latest`

- **Code for data analysis and plotting using NAIL framework:**

  `https://github.com/mthakorecern/PisaHmm/tree/Phase1`

- **Code for calculating total yields:**

  `https://github.com/mthakorecern/Yield_datacards/tree/master`

Bibliography

[1] P. A. M. Dirac, "The quantum theory of the emission and absorption of radiation," *Proceedings of the Royal Society of London. Series A, Containing Papers of a Mathematical and Physical Character*, vol. 114, no. 767, pp. 243–265, 1927.

[2] E. Fermi, "An attempt of a theory of beta radiation. 1." *Z. Phys.*, vol. 88, pp. 161–177, 1934.

[3] S. L. Glashow, "Partial-symmetries of weak interactions," *Nuclear physics*, vol. 22, no. 4, pp. 579–588, 1961.

[4] A. Salam, "Weak and Electromagnetic Interactions," *Conf. Proc. C*, vol. 680519, pp. 367–377, 1968.

[5] S. Weinberg, "A model of leptons," *Physical review letters*, vol. 19, no. 21, p. 1264, 1967.

[6] P. W. Higgs, "Broken symmetries and the masses of gauge bosons," *Physical Review Letters*, vol. 13, no. 16, p. 508, 1964.

[7] F. Englert and R. Brout, "Broken symmetry and the mass of gauge vector mesons," *Physical Review Letters*, vol. 13, no. 9, p. 321, 1964.

[8] C.-N. Yang and R. L. Mills, "Conservation of isotopic spin and isotopic gauge invariance," *Physical review*, vol. 96, no. 1, p. 191, 1954.

[9] H. Fritzsch, M. Gell-Mann, and H. Leutwyler, "Advantages of the color octet gluon picture," *Physics Letters B*, vol. 47, no. 4, pp. 365–368, 1973.

[10] D. J. Gross and F. Wilczek, "Ultraviolet behavior of non-abelian gauge theories," *Physical Review Letters*, vol. 30, no. 26, p. 1343, 1973.

[11] H. D. Politzer, "Reliable perturbative results for strong interactions?" *Physical Review Letters*, vol. 30, no. 26, p. 1346, 1973.

[12] A. Pais and S. Treiman, "How many charm quantum numbers are there?" *Physical Review Letters*, vol. 35, no. 23, p. 1556, 1975.

[13] D. Griffiths, *Introduction to elementary particles*. John Wiley & Sons, 2020.

[14] F. Halzen and A. D. Martin, *Quark & Leptons: An Introductory Course In Modern Particle Physics*. John Wiley & Sons, 2008.

[15] M. Thomson, *Modern particle physics*. Cambridge University Press, 2013.

[16] F. Hasert, S. Kabe, W. Krenz, J. Von Krogh, D. Lanske, J. Morfin, K. Schultze, H. Weerts, G. Bertrand-Coremans, J. Sacton *et al.*, "Observation of neutrino-like interactions without muon or electron in the gargamelle neutrino experiment," *Nuclear Physics B*, vol. 73, no. 1, pp. 1–22, 1974.

[17] G. Arnison, A. Astbury, B. Aubert, C. Bacci, G. Bauer, A. Bezaguet, R. Böck, T. Bowcock, M. Calvetti, T. Carroll *et al.*, "Experimental observation of isolated large transverse energy electrons with associated missing energy at s= 540 gev," *Physics letters B*, vol. 122, no. 1, pp. 103–116, 1983.

[18] M. Banner, R. Battiston, P. Bloch, F. Bonaudi, K. Borer, M. Borghini, J.-C. Chollet, A. Clark, C. Conta, P. Darriulat *et al.*, "Observation of single isolated electrons of high transverse momentum in events with missing transverse energy at the cern pp collider," *Physics Letters B*, vol. 122, no. 5-6, pp. 476–485, 1983.

[19] G. Arnison, A. Astbury, B. Aubert, C. Bacci, G. Bauer, A. Bezaguet, R. Böck, T. Bowcock, M. Calvetti, P. Catz *et al.*, "Experimental observation of lepton pairs of invariant mass around 95 gev/c2 at the cern sps collider," *Physics Letters B*, vol. 126, no. 5, pp. 398–410, 1983.

[20] P. Bagnaia, M. Banner, R. Battiston, P. Bloch, F. Bonaudi, K. Borer, M. Borghini, J.-C. Chollet, A. Clark, C. Conta *et al.*, "Evidence for z0→ e+ e- at the cern pp collider," *Physics Letters B*, vol. 129, no. 1-2, pp. 130–140, 1983.

[21] F. Abe, H. Akimoto, A. Akopian, M. Albrow, S. Amendolia, D. Amidei, J. Antos, C. Anway-Wiese, S. Aota, G. Apollinari *et al.*, "Observation of top quark production in p p collisions with the collider detector at fermilab," *Physical review letters*, vol. 74, no. 14, p. 2626, 1995.

[22] S. Abachi, B. Abbott, M. Abolins, B. S. Acharya, I. Adam, D. Adams, M. Adams, S. Ahn, H. Aihara, J. Alitti *et al.*, "Observation of the top quark," *Physical Review Letters*, vol. 74, no. 14, p. 2632, 1995.

[23] K. Kodama, N. Ushida, C. Andreopoulos, N. Saoulidou, G. Tzanakos, P. Yager, B. Baller, D. Boehnlein, W. Freeman, B. Lundberg *et al.*, "Observation of tau neutrino interactions," *Physics Letters B*, vol. 504, no. 3, pp. 218–224, 2001.

[24] S. Chatrchyan, V. Khachatryan, A. M. Sirunyan, A. Tumasyan, W. Adam, E. Aguilo, T. Bergauer, M. Dragicevic, J. Erö, C. Fabjan *et al.*, "Observation of a new boson at a mass of 125 gev with the cms experiment at the lhc," *Physics Letters B*, vol. 716, no. 1, pp. 30–61, 2012.

[25] G. Aad, T. Abajyan, B. Abbott, J. Abdallah, S. A. Khalek, A. A. Abdelalim, R. Aben, B. Abi, M. Abolins, O. AbouZeid *et al.*, "Observation of a new particle in the search for the standard model higgs boson with the atlas detector at the lhc," *Physics Letters B*, vol. 716, no. 1, pp. 1–29, 2012.

[26] Y. Fukuda, T. Hayakawa, E. Ichihara, K. Inoue, K. Ishihara, H. Ishino, Y. Itow, T. Kajita, J. Kameda, S. Kasuga *et al.*, "Evidence for oscillation of atmospheric neutrinos," *Physical Review Letters*, vol. 81, no. 8, p. 1562, 1998.

[27] Q. R. Ahmad, R. Allen, T. Andersen, J. Anglin, G. Bühler, J. Barton, E. Beier, M. Bercovitch, J. Bigu, S. Biller *et al.*, "Measurement of the rate of ν e+ d$\rightarrow$ p+ p+ e- interactions produced by b 8 solar neutrinos at the sudbury neutrino observatory," *Physical Review Letters*, vol. 87, no. 7, p. 071301, 2001.

[28] P. D. Group, P. Zyla, R. Barnett, J. Beringer, O. Dahl, D. Dwyer, D. Groom, C.-J. Lin, K. Lugovsky, E. Pianori *et al.*, "Review of particle physics," *Progress of Theoretical and Experimental Physics*, vol. 2020, no. 8, p. 083C01, 2020.

[29] L. Evans and P. Bryant, "Lhc machine," *Journal of instrumentation*, vol. 3, no. 08, p. S08001, 2008.

[30] E. Mobs, "The cern accelerator complex. complexe des accélérateurs du cern," Jul 2016, general Photo. [Online]. Available: https://cds.cern.ch/record/2197559

[31] R. Adolphi *et al.*, "The cms experiment at the cern lhc," *Jinst*, vol. 803, p. S08004, 2008.

[32] T. Sakuma, "Cutaway diagrams of CMS detector," May 2019. [Online]. Available: http://cds.cern.ch/record/2665537

[33] P. TRACZYK, "Introduction to CMS. High School Teachers 2015," Jul 2015. [Online]. Available: http://cds.cern.ch/record/2033485

[34] D. Barney, "CMS Detector Slice," Jan 2016, cMS Collection. [Online]. Available: http://cds.cern.ch/record/2120661

[35] C. Collaboration, L. Quertenmont, S. Basegmez, C. Beluffi, G. Bruno, R. Castello, A. Caudron, L. Ceard, C. Delaere, T. Du Pree *et al.*, "" energy calibration and resolution of the cms electromagnetic calorimeter in pp collisions at $\sqrt{s} = 7$ tev," 2013.

[36] V. Khachatryan, D. Anderson, A. Apresyan, A. Bornheim, J. Bunn, Y. Chen, J. Duarte, A. Mott, H. Newman, C. Pena *et al.*, "The cms trigger system," *Journal of Instrumentation*, vol. 12, no. 1, pp. Art–No, 2017.

[37] C. Collaboration, "Technical proposal for the upgrade of the CMS detector through 2020," Tech. Rep., Jun 2011. [Online]. Available: https://cds.cern.ch/record/1355706

[38] L. Rossi and O. Brüning, "Introduction to the HL-LHC Project," *Adv. Ser. Dir. High Energy Phys.*, vol. 24, pp. 1–17, 2015. [Online]. Available: https://cds.cern.ch/record/2130736

[39] D. Contardo, M. Klute, J. Mans, L. Silvestris, and J. Butler, "Technical Proposal for the Phase-II Upgrade of the CMS Detector," Geneva, Tech. Rep., Jun 2015, upgrade Project Leader Deputies: Lucia Silvestris (INFN-Bari), Jeremy Mans (University of Minnesota) Additional contacts: Lucia.Silvestris@cern.ch, Jeremy.Mans@cern.ch. [Online]. Available: https://cds.cern.ch/record/2020886

[40] S. Lehti and V. Karimäki, "Computing methods in high energy physics," *Lecture Notes*, 2010.

[41] J. Baglio and A. Djouadi, "Higgs production at the lhc," *Journal of High Energy Physics*, vol. 2011, no. 3, pp. 1–53, 2011.

[42] A. M. Sirunyan, A. Tumasyan, W. Adam, F. Ambrogi, E. Asilar, T. Bergauer, J. Brandstetter, M. Dragicevic, J. Erö, A. E. Del Valle *et al.*, "Combination of searches for higgs boson pair production in proton-proton collisions at s= 13 tev," *Physical review letters*, vol. 122, no. 12, p. 121803, 2019.

[43] A. M. Sirunyan, A. Tumasyan, W. Adam, T. Bergauer, M. Dragicevic, J. Erö, A. E. Del Valle, R. Fruehwirth, M. Jeitler, N. Krammer *et al.*, "Evidence for higgs boson decay to a pair of muons," *Journal of High Energy Physics*, vol. 2021, no. 1, pp. 1–68, 2021.

[44] C. collaboration *et al.*, "Sensitivity projections for higgs boson properties measurements at the hl-lhc," *CMS PAS FTR-18-011*, 2018.

[45] I. Antcheva, M. Ballintijn, B. Bellenot, M. Biskup, R. Brun, N. Buncic, P. Canal, D. Casadei, O. Couet, V. Fine *et al.*, "Root—a c++ framework for petabyte data storage, statistical analysis and visualization," *Computer Physics Communications*, vol. 180, no. 12, pp. 2499–2512, 2009.

[46] M. Sadiku, K. Eze, and S. Musa, "High-throughput computing," 08 2018.

[47] J. Basney, M. Livny, and T. Tannenbaum, "High throughput computing with condor," *HPCU news*, vol. 1, no. 2, p. 1, 1997.

[48] The ATLAS Collaboration, The CMS Collaboration, The LHC Higgs Combination Group, "Procedure for the LHC Higgs boson search combination in Summer

2011," Tech. Rep. CMS-NOTE-2011-005, ATL-PHYS-PUB-2011-11, 2011. [Online]. Available: https://cds.cern.ch/record/1379837

[49] C. Collaboration and T. Mc Cauley, "Displays of candidate events in which a Higgs boson decays into two muons," Jul 2020, cMS Collection. [Online]. Available: https://cds.cern.ch/record/2720665

[50] D. Bertolini, P. Harris, M. Low, and N. Tran, "Pileup per particle identification," *Journal of High Energy Physics*, vol. 2014, no. 10, p. 59, 2014.

[51] W. Herr and B. Muratori, "Concept of luminosity," 2006. [Online]. Available: https://cds.cern.ch/record/941318

M Sc

ORIGINALITY REPORT

15%	13%	8%	2%
SIMILARITY INDEX	INTERNET SOURCES	PUBLICATIONS	STUDENT PAPERS

PRIMARY SOURCES

1	d-nb.info Internet Source	2%
2	www.zora.uzh.ch Internet Source	1%
3	hdl.handle.net Internet Source	<1%
4	iihe.ac.be Internet Source	<1%
5	pure.royalholloway.ac.uk Internet Source	<1%
6	pure.uva.nl Internet Source	<1%
7	arxiv.org Internet Source	<1%
8	Submitted to Queen Mary and Westfield College Student Paper	<1%
9	publikationen.bibliothek.kit.edu Internet Source	<1%

10	www.roma1.infn.it Internet Source	<1 %
11	A. M. Sirunyan, A. Tumasyan, W. Adam, T. Bergauer et al. "Evidence for Higgs boson decay to a pair of muons", Journal of High Energy Physics, 2021 Publication	<1 %
12	boris.unibe.ch Internet Source	<1 %
13	repozitorij.unizg.hr Internet Source	<1 %
14	digbib.ubka.uni-karlsruhe.de Internet Source	<1 %
15	tel.archives-ouvertes.fr Internet Source	<1 %
16	sro.sussex.ac.uk Internet Source	<1 %
17	assets.cambridge.org Internet Source	<1 %
18	edoc.ub.uni-muenchen.de Internet Source	<1 %
19	The Large Hadron Collider, 2015. Publication	<1 %
20	Submitted to University of Melbourne Student Paper	<1 %

21	etheses.whiterose.ac.uk Internet Source	<1 %
22	en.wikipedia.org Internet Source	<1 %
23	repository.upenn.edu Internet Source	<1 %
24	repozitorij.pmf.unizg.hr Internet Source	<1 %
25	Anke Biekötter, Raquel Gomez-Ambrosio, Parisa Gregg, Frank Krauss, Marek Schönherr. "Constraining SMEFT operators with associated hy production in weak boson fusion", Physics Letters B, 2021 Publication	<1 %
26	fr.scribd.com Internet Source	<1 %
27	pastel.archives-ouvertes.fr Internet Source	<1 %
28	www.iexp.uni-hamburg.de Internet Source	<1 %
29	P A Zyla, R M Barnett, J Beringer, O Dahl et al. "Review of Particle Physics", Progress of Theoretical and Experimental Physics, 2020 Publication	<1 %
30	pt.scribd.com Internet Source	

		<1 %
31	iopscience.iop.org Internet Source	<1 %
32	mediatum.ub.tum.de Internet Source	<1 %
33	Submitted to Indian Institute of Technology, Madras Student Paper	<1 %
34	Springer Theses, 2016. Publication	<1 %
35	Submitted to University of Bristol Student Paper	<1 %
36	Submitted to University of Sydney Student Paper	<1 %
37	William Barletta, Marco Battaglia, Markus Klute, Michelangelo Mangano, Soren Prestemon, Lucio Rossi, Peter Skands. "Future hadron colliders: From physics perspectives to technology R&D", Nuclear Instruments and Methods in Physics Research Section A: Accelerators, Spectrometers, Detectors and Associated Equipment, 2014 Publication	<1 %
38	www.nikhef.nl Internet Source	<1 %

39	Submitted to Royal Holloway and Bedford New College Student Paper	<1 %
40	authors.library.caltech.edu Internet Source	<1 %
41	Submitted to University of Surrey Student Paper	<1 %
42	repositorio.ufrn.br Internet Source	<1 %
43	www.icepp.s.u-tokyo.ac.jp Internet Source	<1 %
44	Herndon, Matthew. "Higgs Boson Searches at the Tevatron", Annual Review of Nuclear Science, 2011. Publication	<1 %
45	Submitted to University of Birmingham Student Paper	<1 %
46	espace.etsmtl.ca Internet Source	<1 %
47	www.repository.cam.ac.uk Internet Source	<1 %
48	www.sussex.ac.uk Internet Source	<1 %
49	yliu.web.cern.ch Internet Source	<1 %

50	Oliver Brüning, Lucio Rossi. "The High-Luminosity Large Hadron Collider", Nature Reviews Physics, 2019 Publication	<1 %
51	Renato Quagliani. "Study of Double Charm B Decays with the LHCb Experiment at CERN and Track Reconstruction for the LHCb Upgrade", Springer Science and Business Media LLC, 2018 Publication	<1 %
52	Springer Theses, 2015. Publication	<1 %
53	digital.lib.washington.edu Internet Source	<1 %
54	docplayer.net Internet Source	<1 %
55	inspirehep.net Internet Source	<1 %
56	mafiadoc.com Internet Source	<1 %
57	pos.sissa.it Internet Source	<1 %
58	repositorio.unesp.br Internet Source	<1 %
59	scholar.smu.edu Internet Source	<1 %

60	worldwidescience.org Internet Source	<1 %
61	M. Koksal. "Model-independent sensitivity estimates for the electromagnetic dipole moments of the top quark at the Large Hadron Collider and beyond", Nuclear Physics B, 2020 Publication	<1 %
62	archive-ouverte.unige.ch Internet Source	<1 %
63	coek.info Internet Source	<1 %
64	digitalcommons.wayne.edu Internet Source	<1 %
65	ediss.uni-goettingen.de Internet Source	<1 %
66	epp.fnal.gov Internet Source	<1 %
67	eprints.gla.ac.uk Internet Source	<1 %
68	link.springer.com Internet Source	<1 %
69	particlephysicist.files.wordpress.com Internet Source	<1 %

70	sg5.tsukuba.jp.hep.net Internet Source	<1 %
71	tesi.cab.unipd.it Internet Source	<1 %
72	tud.qucosa.de Internet Source	<1 %
73	www-cdf.fnal.gov Internet Source	<1 %
74	Djouadi, A.. "The anatomy of electroweak symmetry breaking Tome II: The Higgs bosons in the Minimal Supersymmetric Model", Physics Reports, 200804 Publication	<1 %
75	G. Aad, B. Abbott, J. Abdallah, S. Abdel Khalek et al. " Observation and measurement of Higgs boson decays to with the ATLAS detector ", Physical Review D, 2015 Publication	<1 %
76	Karaca, Koray. "The construction of the Higgs mechanism and the emergence of the electroweak theory", Studies in History and Philosophy of Science Part B Studies in History and Philosophy of Modern Physics, 2013. Publication	<1 %

77	Michael Winn. "Prospects for Quarkonium Measurements in p–A and A–A Collisions at the LHC", Few-Body Systems, 2017 Publication	<1 %
78	V.A. Khoze, A.D. Martin, M.G. Ryskin. "Double-diffractive processes in high-resolution missing-mass experiments at the Tevatron", The European Physical Journal C, 2001 Publication	<1 %
79	arizona.openrepository.com Internet Source	<1 %
80	citeseerx.ist.psu.edu Internet Source	<1 %
81	ddd.uab.cat Internet Source	<1 %
82	etd.gsu.edu Internet Source	<1 %
83	etd.lib.metu.edu.tr Internet Source	<1 %
84	hal-polytechnique.archives-ouvertes.fr Internet Source	<1 %
85	krex.k-state.edu Internet Source	<1 %
86	livrepository.liverpool.ac.uk Internet Source	<1 %

87	nbn-resolving.de Internet Source	<1 %
88	physics.bu.edu Internet Source	<1 %
89	tedhuntington.com Internet Source	<1 %
90	tuprints.ulb.tu-darmstadt.de Internet Source	<1 %
91	Monika Blanke, Priscilla Pani, Giacomo Polesello, Giulia Rovelli. "Single-top final states as a probe of top-flavoured dark matter models at the LHC", Journal of High Energy Physics, 2021 Publication	<1 %
92	Sebastian Baum, Riccardo Catena, Jan Conrad, Katherine Freese, Martin B. Krauss. "Determining dark matter properties with a XENONnT/LZ signal and LHC Run 3 monojet searches", Physical Review D, 2018 Publication	<1 %
93	theses.gla.ac.uk Internet Source	<1 %
94	thesis.library.caltech.edu Internet Source	<1 %
95	Elodie Resseguie. "Electroweak Physics at the Large Hadron Collider with the ATLAS	<1 %

Detector", Springer Science and Business Media LLC, 2020
Publication

96	H. G. Dosch, V. F. Müller. "The facets of relativistic quantum field theory", The European Physical Journal H, 2011 Publication	<1 %
97	Juan Pedro Ochoa Ricoux. "Neutrino Physics", A Search for Muon Neutrino to Electron Neutrino Oscillations in the MINOS Experiment, 2011 Publication	<1 %
98	The Search for the Higgs Boson at CMS, 2013. Publication	<1 %
99	etheses.dur.ac.uk Internet Source	<1 %

Exclude quotes	On	Exclude matches	Off
Exclude bibliography	On		